EXHUMATION AND INCISION HISTORY OF THE TORNGAT MOUNTAINS, NORTHERN LABRADOR AND QUEBEC, CANADA, USING APATITE (U-Th)/He THERMOCHRONOLOGY

by

Juan Pablo Centeno
B.S., University of Kansas, 2001

Submitted to the Department of Geology and the Faculty of the Graduate School of the University of Kansas in partial fulfillment of the requirements for the degree of Master of Science

Redacted Signature

Daniel F. Stockli (Chairman)

Redacted Signature

John C. Gosse

Redacted Signature

Douglas Walker

Date Submitted: _____

ABSTRACT

Juan Pablo Centeno, M.S.

Department of Geology, May 2005

University of Kansas

Apatite (U-Th)/He thermochronological data provide new insights into the exhumation history of the Torngat Mountains, which are located in Ungava Peninsula, northern Labrador and Quebec, Canada. Latest Jurassic to earliest Cretaceous rifting resulted in crustal extension and opening of the Labrador Sea, causing westward tilting and exhumation of the Labrador continental margin. Post-rift erosion and incision led to the formation of significant topographic relief in the Torngat Mountains. Thermal modeling of apatite (U-Th)/He thermochronological data from a vertical sample transect indicates that rapid cooling starting at ~140-150 Ma, which closely coincides in age with independent geological evidence for initial rifting in the area. Apatite (U-Th)/He ages along an E-W transect, which was collected perpendicular to the Torngat Mountains and the Labrador coast, record differential extensional and erosional exhumation diminishing westwards towards the interior of Ungava Peninsula. Ages near the Labrador coastline are as young as ~78 Ma and are significantly younger than the timing of onset of initial rifting (~140-150 Ma); this suggests significant amounts (~1-2 km) of post-rift erosion and incision along the eastern continental margin of the Labrador Sea. West of the Torngat Mountains, along the E-W transect, apatite (U-Th)/He ages also show evidence of substantial post-rift erosion likely related to Mesozoic and Tertiary fluvial erosion or to Pleistocene continental glaciation. Two constant-elevation N-S transects collected parallel to the Labrador coast show apatite (U-Th)/He ages that mimic the larger scale topographic features of the area, such as major rivers and fiords, indicating a deflection of shallow crustal isotherms due to post-rift development of high-amplitude topography. Additional numerical modeling is required to refine the timing and spatial magnitude of post-rift erosion in more detail.

TABLE OF CONTENTS

TABLE OF CONTENTS (CONTINUED)

LIST OF FIGURES AND TABLES

LIST OF FIGURES AND TABLES (CONTINUED)

ACKNOWLEDGEMENTS

I thank the entire faculty and staff of the Department of Geology at the University of Kansas for contributing their time and knowledge to my education in geology throughout my undergraduate and graduate degrees. I am grateful to the members of my thesis committee, Professors Daniel Stockli, John Gosse, and Doug Walker, for their insightful reviews and advice throughout the completion of this thesis. I thank Jane Staiger and James Gray for their help and good company during the field season in the Torngats in the summer of 2002; T.J. Dewane for his help with the ICP-MS at the University of Kansas; and the rest of the staff and students at the Isotope Geochemistry Laboratory for their help in the processing of my samples.

Finally I would like to thank all those good friends that helped me get through grad school. Same goes to my parents and brother who were always there to support me.

PREFACE

This thesis presents the results of a research project conducted during the completion of a Master's degree in Geology at the University of Kansas. It is divided into two chapters followed by two appendices: (1) an introduction to the study; (2) a manuscript which presents an introduction, geological setting, analytical methodology, results, interpretations, discussion, and conclusions of this research project to be submitted to *Tectonics*; (A) a description of the analytical procedures employed in this apatite (U-Th)/He thermochronology study; and (B) a table presenting all the apatite (U-Th)/He age data obtained.

CHAPTER 1:

Introduction

The eastern passive continental margin of northern Labrador, Canada, started developing in the latest Jurassic to earliest Cretaceous due to rifting of the Canadian-Greenland craton. Rifting occurred as a consequence of the northwestward propagation of extension in the North Atlantic Ocean after the break up of Pangea. Along the eastern continental margin of Labrador, topography is characterized by an escarpment and the rugged terrain of the Torngat Mountains (Figures 1 and 2). This is similar to what is observed at recent (e.g. the Red Sea) and older (e.g. southeastern Australia, Brazil, and southwestern Africa) passive continental margins where an escarpment and rugged topography develop due to uplift and exhumation and subsequent erosion of the rift margins (e.g., Ollier, 1984; Bohannon et al., 1989; Gallagher et al., 1994; Kooi and Beaumont, 1994; Bishop and Goldrick, 2000; Brown et al., 2000). We here present the results of a study utilizing (U-Th)/He thermochronology to investigate the exhumation and incision history of the Torngat Mountains to improve our understanding of the exhumation and the topographic development in northeastern Labrador during and subsequent to rifting along the western margin of the Labrador Sea.

The study area occupies parts of northernmost Labrador and Quebec, Canada. It is located in Ungava Peninsula (Figure 2), and is centered approximately at 59°00'N latitude and 64°30'W longitude (Figure 3) and ~450 km north-west of

Kuujjuaq, Quebec. The provincial boundary between Quebec and Labrador is the drainage divide that roughly follows the highest peaks of the Torngat Mountains (Figure 2). Along the eastern half of Ungava Peninsula (roughly east of 64°30'W longitude), topography is characterized by the high (>1500 m) flat-topped peaks and deep U-shaped valleys of the Torngat Mountains. The western half of Ungava Peninsula shows lower elevation topography (~600 m) with considerably less jagged relief than the eastern half (Figure 6). Along the Labrador Sea coast, deep and wide U-shaped valleys dissect the region and terminate in fiords that drain the watershed east of the Torngat Mountains. The geology of Ungava Peninsula is dominated by Precambrian crystalline rocks that were amalgamated and metamorphosed during Paleoproterozoic orogenies (Wardle et al., 2002). Syn- and post-rift strata in the Labrador Sea (Figure 5) are predominantly derived from the erosion of the Labrador and Greenland passive margins (Srivastava et al., 1980; Balkwill et al., 1990), and an increased Quaternary sediment flux from interior Canada in response to continental glaciation (Umpleby, 1979; Srivastava et al., 1980; Piper et al., 1990).

This Master's thesis is the result of collaboration among colleagues from the Department of Geology at the University of Kansas (KU), Department of Earth Sciences at Dalhousie University (DAL), and the Department of Geography at the Université de Montréal (UdeM). Professors John Gosse (DAL) and Daniel Stockli (KU) provided the funding and assisted with sample collection during field work in the summer of 2002. All analytical work was carried out by J. P. Centeno at the (U-Th)/He laboratory in the Isotope Geochemistry Laboratories of the Department of

Geology at the University of Kansas. Professor Gwen Macpherson (KU) and doctoral student T. J. Dewane (KU) assisted in measuring uranium and thorium concentrations using the KU ICP-MS laboratory.

This thesis also builds on research efforts by J. Staiger (Ph.D. at DAL), who is evaluating the generation of relief in the Torngat Mountains produced by Quaternary glacial erosion; and by G. Marquette (former Ph.D. at UdeM), who researched altitudinal weathering contrasts due to Quaternary glaciation in the northern Labrador and Quebec region of northern Canada.

Chapter 2 of this thesis was written in the form of a publishable manuscript that addresses the thermal evolution and exhumation of the western Labrador Sea rift margin in northern Labrador and Quebec, Canada. It represents a collaborative effort with D. Stockli and J. Gosse. This manuscript will be submitted to the journal *Tectonics* for publication.

CHAPTER 2:

Exhumation and Incision History of the Torngat Mountains, Northern Labrador and Quebec, Canada, Using Apatite (U-Th)/He Thermochronology

Abstract

Apatite (U-Th)/He thermochronological data provide new insights into the exhumation history of the Torngat Mountains, which are located in Ungava Peninsula, northern Labrador and Quebec, Canada. Latest Jurassic to earliest Cretaceous rifting resulted in crustal extension and opening of the Labrador Sea, causing westward tilting and exhumation of the Labrador continental margin. Post-rift erosion and incision led to the formation of significant topographic relief in the Torngat Mountains. Thermal modeling of apatite (U-Th)/He thermochronological data from a vertical sample transect indicates that rapid cooling starting at ~140-150 Ma, which closely coincides in age with independent geological evidence for initial rifting in the area. Apatite (U-Th)/He ages along an E-W transect, which was collected perpendicular to the Torngat Mountains and the Labrador coast, record differential extensional and erosional exhumation diminishing westwards towards the interior of Ungava Peninsula. Ages near the Labrador coastline are as young as ~78 Ma and are significantly younger than the timing of onset of initial rifting (~140-150 Ma); this suggests significant amounts (~1-2 km) of post-rift erosion and incision along the eastern continental margin of the Labrador Sea. West of the Torngat Mountains, along the E-W transect, apatite (U-Th)/He ages also show evidence of

substantial post-rift erosion likely related to Mesozoic and Tertiary fluvial erosion or to Pleistocene continental glaciation. Two constant-elevation N-S transects collected parallel to the Labrador coast show apatite (U-Th)/He ages that mimic the larger scale topographic features of the area, such as major rivers and fiords, indicating a deflection of shallow crustal isotherms due to post-rift development of high-amplitude topography. Additional numerical modeling is required to refine the timing and spatial magnitude of post-rift erosion in more detail.

I. Introduction

The Torngat Mountains are located on Ungava Peninsula in northernmost Labrador and Quebec, Canada, along the western continental margin of the Labrador Sea (Figure 2). The mountainous landscape is characterized by steep-sided, mostly flat-topped upland surfaces with average peak elevations of ~1500 m that are dissected by deeply incised U-shaped valleys, cirques, and fiords. Maximum local topographic relief (including fiord bathymetry) exceeds ~2000 m. In contrast, the western half of Ungava Peninsula is dominated by low relief (<500 m), low elevation (~700 m), and rounded topography. Compared to the Canadian Shield to the west and the North American eastern coast to the south, the relief across the Torngat Mountains appears to be anomalously immature (see Figure 1). It is characterized by apparently youthful, short wavelength, and high amplitude topography (λ=~10 km, h_0>1500 m) (Figure 6).

There is no agreement yet on the origin of topography along the western margin of the Labrador Sea. Cooke (1929), McMillan (1973), Gradstein and Srivastava (1980), and Balkwill et al. (1990) believed the Labrador Shelf region has undergone renewed tectonic activity since Neogene time. Hall et al. (2002) and Wardle et al. (2002), based on seismic refraction cross sections, believed topography could be the result of isostasy due to a remnant Paleoproterozoic crustal root (>49 km) related to the Torngat Orogeny.

The purpose of this project is to develop a more quantitative understanding of the geologic and topographic evolution of the Torngat Mountains. The two main goals associated with this project are (1) to determine the exhumation and tectonic history of the Labrador margin and (2) to quantify the topographic evolution of the Torngat Mountains using apatite (U-Th)/He thermochronology.

Thermal histories were determined using apatite (U-Th)/He thermochronometry; a technique based on the α-decay of ^{235}U, ^{238}U, and ^{232}Th series nuclides (e.g., Farley and Stockli, 2002). Apatite (U-Th)/He dating was chosen due to its low thermal sensitivity and its low closure temperature (~75°C) for helium diffusion (e.g., Wolf et al. 1996; Farley 2000). Helium is progressively lost at temperatures between ~40 and ~75°C over geological time; this temperature range is called the He Partial Retention Zone (HePRZ). Vertical sample arrays from boreholes or exhumed intact crustal sections allow the reconstruction of progressive cooling and exhumation histories (Stockli et al. 2001, 2002; Farley 2002). Two vertical sample transects (Mt. D'Iberville and Mt. Inuit) were collected to identify the magnitude,

timing, and rate of exhumation (see Figures 3 and 4 for locations). A ~100 km long east-west transect across Ungava Peninsula (29 samples) was collected to determine exhumational variations across the peninsula and evaluate the amount of rift shoulder rotation (rift flank uplift) (Figures 3 and 4). Stüwe (1994) and Mancktelow and Grasemann (1997) showed how eroding topography influences the shape of isotherms in the shallow crust. Shallow isotherms (<100°C) tend to mimic topographic features such as deep valleys and high ridges. The low-temperature sensitivity of apatite (U-Th)/He dating is key for detecting isotherm deflections that quantify the incision history. For this purpose, we collected two north-south, iso-elevation transects at 450 and 1000 m following the strategy of House et al. (1998).

Given the absence of localized structural discontinuities such as rift-bounding normal faults, we expect to find a systematic (U-Th)/He age-elevation relationship from the two vertical profiles that will allow us to determine the magnitude and rate of long term exhumation, assuming a range of realistic geothermal gradients. From the two north-south equal-elevation transects, we expect to find differences in (U-Th)/He ages that will help us constrain the timing of incision and development of topography. Using this approach, we would expect older (U-Th)/He ages from samples taken from paleo-valleys and younger (U-Th)/He ages from samples taken along paleo-ridges (House et al. 1998, 2001; Ehlers and Farley, 2003). These data combined with the results from both vertical transects and the east-west transect across the entire Ungava peninsula will enable us to differentiate between the two hypotheses which predict that the present rugged topography in northern Labrador

(Torngat Mountains) is either the result of (1) Cretaceous to early Tertiary relief generation associated with rift margin uplift and the opening of the Labrador Sea or (2) renewed isostatically-driven uplift and formation of significant relief in Neogene times. We expect to find systematic variations in (U-Th)/He ages along the east-west transect across Ungava Peninsula that should shed light on the tectonic and topographic evolution of the Torngat Mountains since the onset of rifting. If the Torngat Mountains and Ungava Peninsula represent a classic exhumed rift margin, we predict younger (U-Th)/He ages along the Labrador coast corresponding to higher magnitudes of exhumation trending older farther west, away from the rift margin towards Ungava Bay. However, if the topography of the Torngat Mountains is related to renewed significant Tertiary updoming and incision, we would expect the youngest ages to be found in the core of the range and ages to systematically increase both towards the Labrador Sea and Ungava Bay. Furthermore, the vertical transect (U-Th)/He data will provide constraints on the timing of accelerated cooling along the east-west transect and therefore resolve whether rapid cooling occurred during or after the rifting of the Canadian-Greenland craton to form the Labrador Sea.

II. Geologic and Tectonic Evolution

The Torngat Mountains are located along the northeastern coast of Labrador, Canada, (Figure 2) in the geographic region of Ungava Peninsula. To the west is Ungava Bay, which is a relatively shallow basin partially filled with glacial deposits; to the east is the Labrador Sea, an average depth (~3500 m deep) oceanic basin that

formed due to continental rifting and seafloor spreading between the Canadian-Greenland craton. Kinematically complex and temporally protracted and polyphase rifting and subsequent seafloor spreading occurred between the Early Cretaceous and Oligocene as a result of the northwestern expansion of the North Atlantic Ocean (Hass, 1997).

Ungava Peninsula is composed of Archean fragments and Paleoproterozoic continental, oceanic, and syn-collisional sedimentary deposits that were amalgamated during the assembly of the Canadian Precambrian Shield in the Paleoproterozoic (Wardle et al., 2002). These rocks predominantly comprise high-grade ortho- and para-gneisses (amphibolites, granulites, and migmatites) and minor pegmatites, diabases, and basalts, ranging in age from Archean to Cambrian (Taylor, 1979).

There is very little evidence for Paleozoic activity in the area. Isolated sparse Ordovician limestone, found on land and in boreholes on the Labrador Sea shelf (Little, 1936; Jenkins, 1984; Balkwill et al., 1990), have been suggested to once have belonged to an extensive carbonate platform that covered the Precambrian basement (Balkwill et al., 1990). No other Paleozoic strata or structures have been found.

Regional studies covering the southern Canadian Atlantic (Nova Scotia) and the northern North Atlantic (Baffin Bay, Greenland, and the Norwegian Sea) have detected increased thermal activity during the Mesozoic and Early Cenozoic (Grist et al., 1992; Chalmers et al., 1995). Jurassic sediments offshore Nova Scotia experienced elevated temperatures during the Early Cretaceous, possibly as a result of volcanism (Grist et al., 1992). Chalmers et al. (1995) suggested that the widespread

presence of Paleocene mafic volcanic rocks in Baffin Bay, west Greenland, southeast Greenland, the Norwegian Sea, and northeast England could be the manifestation of a very large (~2000 km) and hot mantle plume head under a thinned lithosphere, which cooled and contracted in the Early Eocene. The present Icelandic plume is thought to represent a remnant of this larger proto-Icelandic mantle plume head. This scenario appears to be supported by the reconstructions of Lawver and Müller (1994) that traced the location of the stem of the Icelandic plume at ~70 Ma to the northeast of the Disko area in west Greenland (~70° N, ~53° W).

Northward extension of the Atlantic Ocean caused rifting on the western and eastern sides of Greenland, resulting in the formation of the Norwegian Sea to the east and the Labrador Sea to the west. In the Labrador region, rifting of the Canadian-Greenland craton started in Early Cretaceous time (Balkwill et al., 1990), ultimately leading to continental rupture and seafloor spreading that lasted from the Early Paleocene to the Early Oligocene (Srivastava, 1978; Chalmers and Pulvertaft, 2001).

The Labrador Sea is on average ~900 km wide and ~3500 m deep. Extensional normal faulting and sedimentation was asymmetrical across the basin (Chalmers and Pulvertaft, 2001). The basin is floored by extensionally attenuated continental crust for ~225 km and by oceanic crust for another ~225 km, up to the extinct spreading axis (see Chalmers and Pulvertaft, 2001). Tertiary transform faults offset the extinct initial spreading axis of the Labrador Sea and caused some reorientation in the spreading direction during the seafloor spreading episode at ~55 Ma (Srivastava, 1978; Chalmers and Pulvertaft, 2001). The passive margins of

eastern Labrador and southwestern Greenland have been eroding since the Cretaceous (Balkwill et al., 1990; Chalmers, 1997). Thick accumulations of Mesozoic and Cenozoic sediments were deposited along the shelves of both margins, with many stratigraphic units extending across the entire basin (Balkwill et al., 1990; Chalmers, 1997).

1. Paleoproterozoic Orogenies

Ungava Peninsula is tectonically part of the Southeastern Churchill Province (SECP) and the Nain craton. The SECP is composed of the New Quebec Orogen, the Core Zone, and the Torngat Orogen (see below for more details on the formation of the SECP). On a regional scale the SECP is located between the Superior and Nain cratons (Figure 2). Both of these cratons are Archean in age and they are both composed mostly of amphibolites, migmatites, and diabases (Taylor, 1979).

The SECP was assembled during the Paleoproterozoic after the collision of the Nain craton (from the east) with the Core Zone, to produce the Torngat Orogen; later, the collision of the Core Zone with the Superior craton (from the west), produced the New Quebec Orogen (Wardle et al., 2002).

Initial collision along the Torngat Orogen occurred between 1.87-1.85 Ga, and produced granulite facies metamorphism and the Torngat crustal root. The root is ~50 km deep and lies approximately 15 km west underneath the Torngat Mountains (Funck and Louden, 1999; Funck et al., 2000; Hall et al., 2002; Wardle et al., 2002).

After the initial collision, a period of transpressional deformation followed from 1.85-1.82 Ga and produced the Abloviak Shear Zone (Figure 2; Wardle et al., 2002).

The New Quebec Orogen developed between 1.82-1.77 Ga and stresses were transmitted through the interior of the SECP. This produced transpressional deformation (George River and Lac Tudor shear zones; see Wardle et al., 2002) that reached the Torngat Orogen to produce the Komaktorvik shear zone (Figure 2; Wares and Goutier, 1990; Wardle et al., 2002).

The youngest Proterozoic rocks in the area are approximately 1.1 Ga old (Taylor, 1979). There are a few Cambrian diabase dikes and some Ordovician dolomites found on land and in the Labrador Sea basin (Balkwill et al., 1990). The lack of a rock record from the Late Proterozoic up to the Mesozoic suggests that the area has been extensively eroded during these times and later. It is also probable that the Paleozoic remnants in the Ungava Peninsula region once belonged to a widespread platform that covered the Precambrian basement. This platform was eroded prior to and during Early Cretaceous rifting of the Canadian-Greenland craton (Balkwill et al., 1990).

2. The Labrador Sea: Meso-Cenozoic Basin Development

The offshore record in the Labrador Sea, as presently sampled by seismic and well data, dates back to the Berriasian (Early Cretaceous). A phase of Early Cretaceous rifting in the Canadian-Greenland craton is evidenced by the emplacement of continental volcanic rocks (basalts) of the Alexis Formation (139-104 Ma;

Umpleby, 1979), northwest normal faulting on Precambrian basement rocks (Balkwill et al., 1990), and the deposition of the predominantly non-marine, coarse-grained arkosic sandstones of the Bjarni Formation (Umpleby, 1979), which was deposited in northwest-striking grabens and half-grabens in Precambrian basement (Figure 5; Balkwill et al., 1990).

This early rifting stage along the Labrador margin was characterized by normal faulting and the deposition of coarse-clastic sediments. The Bjarni Formation is confined to the proximal part of the Cretaceous succession of the Labrador shelf and it has been given maximum and minimum ages of Barremian to Coniacian (~125-87 Ma) (Umpleby, 1979; McWhae et al., 1980) (Figure 5). It is overlain by the Freydis Member of the Markland Formation, another syn-rift deposit, part of the inner shelf, a Late Cretaceous unit, with ages ranging from Coniacian to Maastrichtian (~87-68 Ma). The Freydis Member of the Markland Formation shows a shallow marine to non-marine depositional environment of predominantly sandstones (Balkwill et al., 1990).

The marine shales of the Markland Formation overlie the Freydis Member and are also within the inner shelf succession (Figure 5); these were deposited during the transition from rifting to drifting in the Labrador Sea (Balkwill et al., 1990). In the innermost shelf regions, the shales are coeval or grade into the Freydis Member. The shales range in age from Coniacian to Late Paleocene (~87-60 Ma) and they have been interpreted to represent a shallow marine environment (Balkwill et al., 1990).

Chalmers and Laursen (1995) concluded that seafloor spreading in the Labrador Sea began during Chron 27, approximately 61 Ma ago. Around that time period, deposition of the Cartwright Formation extended into the inner and outer parts of the Lower Tertiary shelf (Figure 5). The Cartwright Formation is predominantly composed of marine shales that range in age from Paleocene to Early Eocene (~60-50 Ma) (McWhae et al., 1980; Balkwill et al., 1990). It is in lower contact with seafloor-spreading submarine Paleocene volcanics (Figure 5).

At approximately 55 Ma, a reorientation of the spreading axis of the Labrador Sea occurred due to the initiation of seafloor spreading between Europe and Greenland (Chalmers and Pulvertaft, 2001). As a result, there is a discordance of about 13° between anomaly 25n, which trends ~N27°W, and anomaly 24n, which trends ~N40°W in the central part of the Labrador Sea (see Chalmers and Pulvertaft, 2001).

The Cartwright Formation is overlain by a thick and widespread, shale-dominated, marine succession of the predominantly Eocene (~50-30 Ma) Kenamu Formation (McWhae et al., 1980; Balkwill et al., 1990). The middle and upper members extend underneath the Labrador continental slope and continue to the Greenland continental shelf (Figure 5). The most striking characteristics of this formation are the general tendencies for upward fining of the lower member and upward coarsening of the middle and upper members, which indicates general subsidence during the lower member deposition and gradual shallowing during progradation of the middle and upper members (Balkwill et al., 1990). The

shallowing trend in the middle and upper members is related to the cessation of seafloor spreading at ~33 Ma (Srivastava, 1978) and culminates with a regional unconformity in the uppermost surface of the Kenamu Fm.

Around the time seafloor spreading ended, the Mokami Formation was deposited, also extending onto the Greenland continental shelf (Figure 5). The Mokami Fm. has an age range from Early Oligocene to Late Miocene (~30-10 Ma; McWhae et al., 1980) and is composed of a lower shale-dominated member and an upper sand member (Balkwill et al., 1990). It coarsens upward and landward and overlies the unconformity above the Kenamu Formation. Coarse grained quartz and igneous clasts from the upper Mokami member are evidence for a period of uplift along coastal Labrador in the Late Oligocene to early Miocene (Balkwill et al., 1990). This coincides in time with a poorly documented uplift event along the central west Greenland margin (Chalmers, 2000).

Above the Mokami Fm., the Saglek Formation has an age range from Early Miocene to Late Pliocene (~22-2 Ma) and was deposited as two members separated by a regional unconformity. The lower member is a conglomeratic sandstone intercalated with the Mokami Fm. along the Labrador shelf. The upper member is a conglomerate (Balkwill et al., 1990), also intercalating with the Mokami Fm. along the Labrador continental slope. The unconformity can be traced across the Labrador Sea (Grant, 1980; Balkwill et al., 1990) and it may mark a major uplift event along the coastal regions.

Following the deposition of the Saglek Formation, the entire Labrador Shelf is dominated by sedimentation of Pleistocene glacial deposits. Three glacial drift units have been identified: Lower till, Upper till, and Hudson Strait till (Piper et al., 1990). These units were deposited during advances and retreats of glaciers during the Pleistocene. This is followed by deposition of the Qeovik silt, a post glacial deposit, believed to have a distant provenance due to the abundance of limestone which is absent in the Labrador area (Piper et al., 1990). Finally this is followed by the deposition of Holocene post-glacial marine sediments: Makkay clay, Sioraq sand, and continental slope sediments (Piper et al., 1990).

III. Methods

Apatite (U-Th)/He thermochronology is a technique used to reconstruct low-temperature (<100°C) thermal histories for upper crustal rocks. Similar to apatite fission track thermochronology, this technique has been used to determine temperature histories and denudation rates of rifted margins (e.g., Persano et al 2002; Spotila et al., 2004). The low closure temperature of the apatite (U-Th)/He system (~75°C) also makes it suitable for determining topographic evolution. Stüwe (1994) and Mancktelow and Grasemann (1997) showed how eroding topography influences the shape of isotherms in the shallow crust and how the magnitude of isotherm deflection increases as they get closer to the surface. The low closure temperature of the apatite (U-Th)/He system makes it the most suitable tool in detecting the deflection of crustal isotherms due to topographic cooling.

The apatite (U-Th)/He technique can be applied to estimate temperature history and denudation rates of rifted margins, providing a means of assessing the timing and volume of sediment being delivered to sedimentary basins. The low closure temperature of this system allows denudation of the earth's surface as low as 2 km to be detected. Several studies have succeeded in implementing this technique to date and quantify exhumation in different geologic settings (House et al., 1998; Stockli et al., 2000; Farley et al., 2001; Persano et al., 2002; Pik et al., 2003; Spotila et al., 2004).

1. Apatite (U-Th)/He Thermochronology

The basis for (U-Th)/He dating is the production of ^{4}He nuclei (α-particles) from the decay of ^{235}U, ^{238}U, and ^{232}Th. On the basis of the He ingrowth equation, (U-Th)/He ages can be determined as a function of ^{4}He, U, and Th concentrations in samples (e.g., Wolf et al., 1996; Farley, 2002; Farley and Stockli, 2002). Apatite crystals quantitatively retain He at temperatures below 40°C and diffusively lose all He at temperatures above ~75°C (Wolf et al., 1996; Farley, 2000; Farley, 2002; Farley and Stockli, 2002). At temperatures between 40°C and ~75°C, partial He retention is extremely temperature-sensitive and (U-Th)/He ages could vary by millions of years over very small vertical increments (Farley, 2002). This temperature zone is called the Helium Partial Retention Zone (HePRZ) (e.g., Wolf et al., 1998; Farley, 2002; Farley and Stockli, 2002). Additionally, due to long α-stopping distances of U and Th in an apatite crystal, (U-Th)/He ages have to be corrected for

initial α-particle ejection during He production by a factor (F_T) that depends mostly on apatite crystal dimensions (Farley et al., 1996). Apatite (U-Th)/He thermochronometry was carried out following the technique described by Stockli et al. (2000).

2. Passive Margins and Thermochronology

Passive continental margins are formed within a regional extensional environment dominated by crustal thinning and subsidence where the margins are uplifted with respect to the subsiding basin (e.g., Ollier, 1984; Kooi and Beaumont, 1994; van der Beek et al., 1994). A complete model for continental margin development should include information on the subaerial topographic evolution of the margin as well as the sedimentation and subsidence history of the adjacent basin (e.g. Rohrmann et al., 1996). Since some of the subaerial topography is lost due to erosion and only estimates on erosion rates or timing of erosional events can be determined from sediments in the basin, low temperature thermochronometry is a powerful means of quantifying the spatial and temporal distribution of onshore denudation (see Gallagher et al., 1998; Gunnell, 2000). Several studies using the apatite fission track technique (closure temperature of ~110°C) have been successful in dating and quantifying the amount of erosion at passive margins (e.g., Gallagher et al., 1994; Gallagher and Brown, 1997; Gallagher et al., 1998; Brown et al., 2002; Juez-Larré and Andriessen, 2002; Lisker, 2002). Due to the lower closure temperature (~75°C) of

the apatite (U-Th)/He system, smaller amounts of denudation can be detected compared to the apatite fission track technique.

Two models for the evolution of passive margins that are suitable for this study have been described by Kooi and Beaumont (1994), Gallagher et al. (1998), and Gunnell (2000): (1) The scarp retreat model is characterized by a steep escarpment (10°-15° slope) at the continental margin where progressive denudation causes the escarpment to retreat (Figure 7a). Maximum vertical denudation (500-1000 m/Myr) occurs immediately seaward of the scarp edge, the coastal region is characterized by moderate denudation rates (10-20 m/Myr), and the interior by much lower rates (<10 m/Myr). This model produces a strong gradient in apatite (U-Th)/He ages with the oldest ages occurring inland of the scarp and decreasing towards the coast (Figure 7).

A recent thermochronological study by Spotila et al. (2004) across the Blue Ridge escarpment of the Appalachian Mountains (Eastern North America) shows many of the characteristics of the scarp retreat model. Spotila et al. (2004) constructed a forward kinematic model which tracked the position of imaginary apatite (U-Th)/He samples during retreat and lowering of an escarpment subject to slow and regional exhumation. The results from their model mimic the observed pattern of apatite (U-Th)/He ages and show an increase in ages from the coastal plain to the upland surfaces, as well as low exhumation rates at the coast and behind the scarp edge, and high exhumation rates at the scarp edge.

(2) The pinned divide model (Gilchrist et al., 1994; Kooi and Beaumont, 1994) combines a steep escarpment at the margin with a preexisting (antecedent)

drainage divide inland of the initial escarpment. The inland drainage divide causes rapid incision by streams between the escarpment and the drainage divide. This results in a wearing down of the scarp instead of a retreat (Figure 7b). Additionally, if the base level of the rivers draining inland of the preexisting drainage divide is lowered, then a significant amount of denudation will occur inland of the drainage divide. In this case, the scarp will form at the location of the preexisting drainage divide and will be "pinned" at that position (Figure 7b). The model predicts increasing (U-Th)/He ages moving inland from the margin, reaching a maximum at the scarp, and then decreasing further inland (Figure 7).

Persano et al. (2002) found some characteristics of the pinned divide model in the development of the Great Escarpment of southeastern Australia. In their study, theoretical apatite (U-Th)/He ages were calculated using a forward numerical approach for the escarpment retreat and pinned divide models in two scenarios: rapid erosion following break-up and constant slow erosion since break-up. The observed apatite (U-Th)/He ages require that the erosion of the escarpment and the generation of the low elevation coastal region occurred rapidly after break-up, and had to be followed by a period of landscape stability and low erosion rates (Persano et al., 2002). Rapid post-break-up escarpment retreat followed by stabilization is a feature of pinned divide models (Kooi and Beaumont, 1994). Break-up results in an abrupt drop in base level for the rivers flowing to the new ocean, causing rapid river incision and retreat of the escarpment to the drainage divide where the escarpment stabilizes (Persano et al., 2002).

These two models, escarpment retreat and pinned divide, are not likely to be exclusive, but rather represent the two end members of a continuum of possible combinations that will depend on factors such as antecedent topography, location of preexisting drainage divides, response of the lithosphere to denudational unloading, lithological contrasts, and climate controls (Kooi and Beaumont, 1994).

IV. Results and Observations

Samples for apatite (U-Th)/He analysis were collected along three longitudinal transects and two vertical profiles. The rocks collected comprise Precambrian gneisses, amphibolites, and migmatites. Approximately 5 kg of rock per sample were collected. Due to the remoteness of the region, helicopter assistance was needed for the collection of samples approximately across 300 km of terrain.

The apatite (U-Th)/He age data used for this study is summarized in Table 1; all age errors are quoted at $\pm 2\sigma$ (see Farley et al., 2001). A total of 76 samples were collected and separated, with 54 samples containing sufficient and suitable apatite for (U-Th)/He dating. Of these 54 samples, 48 yielded internally reproducible results from at least 3 analyzed aliquots (see Appendix B). Appendix B is a summary of all the (U-Th)/He age analyses carried out in the (U-Th)/He laboratory at the University of Kansas.

Two vertical profiles were sampled in line with a horizontal E-W transect across Ungava Peninsula (see Figures 3 and 4 for locations): a first profile was

collected at Mt. D'Iberville (196 to 1383 m in elevation), and a second profile at Mt. Inuit (251 to 1461 m in elevation).

In addition, three horizontal transects were collected from across the Torngat Mountains (see Figures 3 and 4 for locations). An E-W transect, approximately 90 km long, was collected across the entire Ungava Peninsula and the Torngat Mountains at roughly 59°N latitude, with sample elevations ranging from 16 to 552 m. A ~N-S transect, approximately 140 km long, was collected roughly parallel to the Labrador coast at a constant elevation of ~450 m and approximately 30 km west of the Labrador coastline. A second ~N-S transect, approximately 60 km long and 20 km west of the 450 m ~N-S transect, was collected parallel to the Labrador coast at an approximate constant elevation of 1000 m.

1. E-W Transect Across the Torngat Mountains

The E-W transect was collected across Ungava Peninsula and the Torngat Mountains roughly at 59°N latitude along Nachvak Fiord and west towards Ungava Bay. Samples along the E-W transect were collected at elevations below 560 m.

Apatite (U-Th)/He ages range from 116.7±4.4 Ma at the Labrador coast up to 245.8±37.5 Ma at the west foot of the Torngat Mountains (Figure 8). The transect shows a pattern of increasing apatite (U-Th)/He ages moving in a westerly direction, away from the Labrador coast, up to ~15 km west of the highest peaks of the Torngat Mountains. Apatite (U-Th)/He ages then decrease going further west towards Ungava Bay but are significantly older than the samples from along the Labrador coast

(Figure 8). A topographic profile along the transect (Figure 8) illustrates a Labrador coastal region with an average elevation of ~400 m, the Torngat Mountains with an average elevation of ~1200 m, and interior Ungava Peninsula with an average elevation of ~600 m. A best-fit age trend through the data illustrates the parabolic pattern of apatite (U-Th)/He ages along the E-W transect showing a fairly constant age trend (~120 Ma) towards the eastern end (Figures 8 and 9).

2. Mt. D'Iberville Vertical Transect

The Mt. D'Iberville vertical profile was collected along the middle of the E-W transect, on the south side of the valley, towards the inland end of Nachvak Fiord, as part of our strategy for determining the amount and timing of exhumation as well as the geometry of exhumation across Ungava Peninsula. The Mt. D'Iberville vertical profile shows a positive correlation of (U-Th)/He ages with elevation (Figure 10) with ages varying from 121.2±8.2 Ma at 196 m to 158.2±3.9 Ma at 1383 m (Table 1). Samples 02-TG-27 and 02-TG-71 gave anomalously high ages and low (U-Th)/He age reproducibility (see Appendix B). These two samples are suspected of having mineral inclusions enriched in U and Th, and are thus excluded from interpretation (see Farley and Stockli, 2002). For a difference in elevation of ~1200 m, the difference in (U-Th)/He ages is ~50 Ma. A best fit curve through the data shows a nearly linear function (Figure 10).

3. Mt. Inuit Vertical Transect

The Mt. Inuit vertical profile was also collected along the middle of the E-W transect, on the north side of the valley, towards the inland end of Nachvak Fiord and west of the Mt. D'Iberville profile. It was also collected as part of our strategy for determining the amount and timing of exhumation as well as the geometry of exhumation across Ungava Peninsula.

Six samples were collected at elevations ranging from 251 to 1461 m. From these samples, only three contained suitable apatite to be dated. Two of those samples, 02-TG-35 and 02-TG-59 yielded ages with low internal reproducibility with best age estimates of ~260 Ma and ~233 Ma, respectively (see Appendix B). Sample 02-TG-58 yielded an age of 220.1±19.1 Ma. These results from Mt. Inuit suggest an inverse correlation between elevation and apatite (U-Th)/He age. Due to poor quality of apatite from pelitic para-gneisses and low internal reproducibility of (U-Th)/He ages, the results from the Mt. Inuit profile are presented here, but are not further discussed or used for the quantitative assessment of the exhumation history along the east-west traverse (Appendix B).

4. N-S Transect at 450 m Elevation

Approximately 30 km west of the Labrador coastline the 450 m N-S transect runs roughly parallel to the coast up to latitude 59° 30'N, where the transect takes a NE turn in order to maintain the equal-elevation sampling trend (see Figures 3, 4, and 14). Samples were collected at an approximate elevation of 450 m. The apatite (U-

Th)/He ages range from 78.7±14.3 Ma to 332.6±45.9 Ma. (U-Th)/He ages are relatively older at the southern end of the transect (Saglek Fiord) and trend younger as they approach Nachvak Fiord. Apatite (U-Th)/He ages then increase across Komaktorvik River and finally decrease again at Kangalaksiorvik Fiord as they approach the northern end of the transect (Figure 14). The apatite (U-Th)/He ages follow a decaying sinusoidal curve that is superimposed on a background age trend defined by the E-W transect due to the slight obliquity of the N-S transect. The sinusoidal trend in the vicinity of Nachvak Fiord and Komaktorvik River has a wavelength of ~74 km (Figure 15). The average wavelength of major topographic features along the 450 m N-S transect is approximately 20 km. A larger wavelength of ~40 km can be seen between the main drainages (i.e. Kangalaksiorvik, Nachvak Fiord, Korok River, and Saglek Fiord) (Figure 15). Additional statistical evaluation of the frequency content of the topography using power spectral analysis of digital elevation models is required to determine the existence of a long-wavelength topographic signal (>40 km) that corresponds to the sinusoid wavelength (~70 km) observed in the (U-Th)/He data.

5. N-S Transect at 1000 m Elevation

A second N-S sample transect was collected at ~1000 m and is located ~20 km west of the 450 m transect, running roughly parallel to the Labrador coastline and down the axis of the Torngat Mountains. The apatite (U-Th)/He ages range from 143.9±5.8 Ma to 233.2±56.9 Ma (Figure 16). Out of the eleven samples collected,

only nine samples produced good quality data. Samples 02-TG-57 and 02-TG-60 yielded anomalously old and internally irreproducible results, ranging from ~570 to ~1920 Ma (see Appendix B).

The along-strike variations in (U-Th)/He ages at 1000 m can be characterized and interpreted in two fundamentally different ways: (1) a near-horizontal linear fit through the data with significant random scatter about the mean at ~200 Ma (Figure 16), or (2) a systematic sinusoidal curve fit with a wavelength of ~34 km (Figure 17), which is roughly half of the 450 m age wavelength. Unfortunately, the quality and density of available data do not allow for a differentiation between these two possible along-strike fits.

Power spectral analysis were calculated from one-dimensional topography along the 1000 m transect using a forward Fast Fourier Transform approach to evaluate the dominant wavelengths of topographic relief in drainages orthogonal to the Labrador Sea coast (Figure 18). The power spectrum is defined as the square of the linear spectrum magnitude and indicates the power of each frequency component. Analysis of the one-dimensional topography along the 1000 m transect shows significant topographic wavelengths of ~31, ~25, ~20, and ~10 km; with the ~31 and ~10 km topographic signals representing the two dominant wavelengths (Figure 18). In logarithmic space, the power appears to approximate a straight line, which indicates that the topography displays fractal properties, meaning the topography is scale-invariant (Figure 18). Visual inspection of the topographic profiles supports the power spectral analysis, suggesting a distance between major drainages ranging from

~25-30 km (i.e. between latitudes 59°00'N and 59°15'N) and a wavelength of ~10 km for smaller topographic features (Figure 17). In order to asses the powers of wavelengths >35 km, longer one-dimensional topographic data arrays will have to be evaluated by either picking a longer baseline or by stringing together parallel profiles in x direction.

V. Interpretation of (U-Th)/He Data

In the following sections, the implications of the apatite (U-Th)/He data from the various sample transects are discussed in detail. The vertical transect from Mt. D'Iberville is strategically collected in-line and is part of the E-W horizontal transect across the Torngat Mountains and Ungava Peninsula. The interpretation and the forward numerical modeling of the vertical transect allow for the quantitative evaluation and interpretation of the latitudinal transect. The two iso-elevational transects parallel to the Torngat Mountains are discussed separately in terms of their implications for the post-rift erosion and incision history and shed light on the timing and nature of landscape evolution and relief generation in the Torngat Mountains.

1. Mt. D'Iberville Vertical Transect

The nearly linear trend and limited increase in (U-Th)/He ages with increasing elevation (Δz = 1200 m) at Mt. D'Iberville suggests that this profile does not represent an exhumed static fossil apatite HePRZ and does not reflect a protracted cooling history, but rather suggest a crustal profile that underwent rapid cooling and

exhumation (Figure 10). The nearly invariant ages from the Mt. D'Iberville profile between 945 and 437 m (~142 Ma) are interpreted to mark the onset of rapid cooling and only trend younger near the bottom of the age-elevation profile due to subsequent erosional cooling.

Numerical forward modeling of possible temperature histories for vertical sample arrays, using laboratory-derived He diffusivity data, were compared with observed age data from the Mt. D'Iberville vertical transect (Figure 11). In this approach, an assumed T-t history is used to calculate the apparent apatite (U-Th)/He age for a specific grain size, diffusivity, and activation energy. Applied forward modeling allows for modeling of individual samples as well as sample arrays from different elevations/depths or temperatures. For this purpose, the observed age-elevation data from Mt. D'Iberville were converted into an age-temperature trend based on elevation differences from the structurally highest sample (02-TG-72), assuming a geothermal gradient of 25°C/km and no significant crustal tilting (Figure 11). The 25°C/km geothermal gradient is an upper limit based on modern heat flow data and chosen to represent a thermal regime that was likely characterized by higher heat flow in the Mesozoic (Barron, 1983; Costain and Speer, 1988; DeConto et al., 1999).

Figure 12 shows realistic temperature-time paths used for forward modeling of Mt. D'Iberville (U-Th)/He transect age data. The displayed temperature-time paths represent only those of the structurally highest sample (02-TG-72), while structurally deeper samples from within the vertical transect sample array were modeled with a

temperature offset proportional to their relative elevation difference. Realistic temperature-time paths were determined iteratively by trial and error. Thermal histories (>80°C) are constrained by older apatite (U-Th)/He ages from the core of the Torngat Mountains (~240-300 Ma) and apatite fission track age data (~275 Ma) (A. Grist, unpublished data).

Figure 12 shows predicted age-paleotemperature curves for model runs 1 through 6. Predicted ages for model runs 1 through 3 yield age patterns that encompass the upper portion of the Mt. D'Iberville age profile, but fail to capture the lower half of the Mt. D'Iberville transect, predicting ages that are significantly younger than the observed data. This behavior is most easily explained by either underestimating syn-rift cooling or overestimating post-rift cooling/erosion. In contrast, model runs 4 through 6 yield predicted age profiles that are in excellent agreement with the observed age-elevation pattern. The temperature-time paths (4-6) are very similar to each other and are characterized by very rapid cooling through the apatite (U-Th)/He partial retention zone starting at ~150 Ma and only slightly differ at very low temperatures. The results are indicative of rapid rift-related cooling during the latest Jurassic to Early Cretaceous and limited post-rift cooling/erosion. Figure 13 presents best-fit temperature-time paths for the vertical sample array from Mt. D'Iberville (model run 5). Results indicate that the entire transect underwent rapid cooling from >80°C to <40°C between ~150-140 Ma. Final erosional exhumation and cooling to mean annual surface temperature are unconstrained by forward modeling, but are limited to <35°C for the structurally deepest sample and <5°C for the

structurally highest sample since ~140 Ma. The timing of rapid cooling appears to be in good agreement with geological evidence for extensional faulting in the latest Jurassic and earliest Cretaceous as suggested by rift-related basaltic volcanism and syn-extensional conglomerate deposition (Balkwill et al., 1990).

2. E-W Transect Across the Torngat Mountains

The latitudinal transect across Ungava Peninsula shows a very systematic trend in (U-Th)/He ages that resembles a positive parabolic curve that is characterized by the oldest ages (>200 Ma) in the core of the Torngat Mountains (Figures 8 and 9). Near the modern-day coastline of eastern Ungava Peninsula, (U-Th)/He ages range from 100 to 150 Ma (Figure 8). Due to postulated westward tilting experienced by the Labrador margin during the rifting process (Hellinger et al., 1983; Lister et al., 1986; Bell et al., 1988), greater distance to the east means increasing paleodepth, resulting in a decrease in (U-Th)/He ages that should become nearly invariant below (i.e. east) of the position of the ~75°C paleoisotherm. The non-marine coarse-clastic conglomerates of the Bjarni Formation (125-87 Ma) were deposited within grabens controlled by large normal faults that run along the eastern margin of the Labrador coast (Balkwill et al., 1990) (Figure 5). Their age of deposition agrees well with the timing of rifting and marks the influx of coarse-clastic sediments during rapid exhumation and syn-rift erosion experienced by the Labrador margin (Figure 9).

Although the Mt. D'Iberville vertical transect indicates that rocks along the western Torngat Mountains underwent rapid cooling due to the rifting process that

created the Labrador Sea starting at ~150-140 Ma, (U-Th)/He ages trend younger at the base of Mount D'Iberville and near the coast approach values of ~122 Ma in Nachvak Fiord and ~78 Ma farther north in Kangalaksiorvik Fiord (Figures 4, 8, and 9). These younger ages are interpreted to reflect moderate post-rift cooling in response to erosional denudation of the Labrador rift flank. Utilizing modeling results of samples from the basal portion of the Mt. D'Iberville transect, these younger ages indicate up to ~30°C of cooling suggestive of <~1.5 km of Mesozoic and Cenozoic post-rift erosion. The most reliable independent constraints on the timing of rapid syn- to post-rift erosion are provided by coarse-clastic rift-basin deposits in the Labrador Sea, such as the Bjarni Fm. (~125-87 Ma) or upper Mokami Fm. (~30-10 Ma).

The relatively rapid increase of (U-Th)/He ages towards the core of the range along the E-W transect appears to represent part of an exhumed pre-rift apatite HePRZ (Figure 9). (U-Th)/He ages as old as ~250 Ma in the core of the range suggest that the Torngat Mountains are largely an erosional remnant of the Labrador rifted margin and do not represent a young Cenozoic mountain range. Along the western flank of the Torngat Mountains, (U-Th)/He ages trend younger and suggest larger amounts of Mesozoic or Cenozoic post-rift cooling and erosional exhumation as a result of fluvial erosion and potentially late Neogene glacial processes.

3. N-S Transect at 450 m Elevation

To constrain the timing of incision and relief generation in the Torngat Mountains, longitudinal transects at constant elevation were collected. A transect was collected roughly parallel to the Labrador Coast at a near constant sampling elevation of ~450 m. The southern part of this transect (Saglek Fiord) is about 10 km farther inland than the 450 m N-S samples in the vicinity of Nachvak Fiord (Figures 3 and 4), which are about 30 km from the coast. This slight obliquity of the transect with respect to the NW-SE trending coastline likely explains older ages (~286 Ma) at the southern end compared to samples around Nachvak Fiord (~136 Ma). At the northern end of the transect, the two northernmost samples were collected only ~13 km west of the Labrador coastline and show some of the youngest (U-Th)/He ages along the transect (115.7 and 78.7 Ma) (Figures 4 and 14). This slight obliquity is manifested in a relatively linear residual trend of increasing ages from N to S as a function of increasing distance from the coastline. Superimposed on this trend is the observed sinusoidal age progression that is interpreted to be a function of incision and topographic cooling.

A power spectral analysis to quantify the importance of this long-wavelength component is in progress. However, analysis of age data from the Nachvak area (Figure 15) shows a wavelength of this sinusoidal variation for (U-Th)/He ages vs. N-S position of ~74 km, which corresponds to the topographic wavelength between major drainage systems, such as the Saglek and Nachvak Fiords (~79 km) (Figure 15). Given this apparent similarity in large-scale wavelength, we propose a causal

correlation between the larger scale topography and the trend in (U-Th)/He ages seen along this transect. The higher frequency topography (e.g., λ=10km) is not detected by our samples; a fact probably related to insufficient sample density (~15 km between samples) along strike or more likely because the higher frequency topography is much younger.

4. N-S Transect at 1000 m Elevation

In general, the (U-Th)/He ages obtained from the 1000 m transect are older than the (U-Th)/He ages from the 450 m transect. This is in good agreement with both observations from the E-W transect and the Mt. D'Iberville transect showing that (U-Th)/He ages get older with increasing distance from the coast towards the core of the Torngat Mountains and increasing elevation, respectively. The fact that these samples were collected at a higher elevation also contributes for these ages being older.

As illustrated by Stüwe (1994) and Mancktelow and Grasemann (1997), topographic cooling induced by the generation of erosional relief influences the shape of isotherms in the shallow crust. Since all these samples are from a constant elevation, the change in (U-Th)/He ages is interpreted as the deflection of crustal isotherms due to topographic cooling. A best-fit curve through the (U-Th)/He data exhibits a wavelength of ~34 km (Figure 17), which is comparable to the large-scale wavelength seen in the topography in the Torngat Mountains between latitudes ~59°00'N and 59°15'N (λ=~36 km) (Figures 16 and 17). Older (U-Th)/He ages are located in the core of the upland surfaces between major drainages and younger (U-

Th)/He ages are located in the vicinity of major drainages (Figure 17). This correlation indicates that the larger scale topography in the area can be seen in the (U-Th)/He data, just as seen for the 450 m N-S transect. This interpretation suggests that only large wavelength topographic features are detectable by apatite (U-Th)/He thermochronometry suggesting short-wavelength topography is superimposed on older drainages. Greater sampling density is needed in order to capture all possible disturbances to the crustal isotherms and test this hypothesis.

VI. Discussion

The older ages at the southern end of the 450 m N-S transects are not associated with any significant changes in lithology or changes in Precambrian terrains. The 450 N-S transect runs parallel to the Abloviak Shear Zone and has been collected along the Precambrian Torngat Orogen as well as along the same lithological unit (Aphebian Granulite; Figure 4) with the exception of a handful of samples that cross into other lithologies. There is no evidence along the 450 m N-S transect that changes in (U-Th)/He ages are affected by lithology or Precambrian terrain.

The general trend of older (U-Th)/He ages towards the south from the 450 N-S transect could either be related to the obliquity of the sample transect with respect to the coastline and paleoisotherms or could alternatively indicate a component of along-strike differential exhumation experienced by the Labrador continental margin. In central west Greenland, Chalmers (2000) presented evidence for uplift in Neogene

times similar to uplift documented in Scandinavia caused by the emplacement of the Icelandic plume (Japsen and Chalmers, 2000). Japsen and Chalmers (2000) suggested the North Atlantic region has undergone two periods of uplift and exhumation in the Cenozoic. Postulated Cenozoic updoming affecting almost the entire North Atlantic region might be invoked to explain possible southward tilting and differential along-strike exhumation of the Labrador continental margin. This might also be consistent with increased sedimentation rates during the late Tertiary (Gradstein and Srivastava, 1980; Balkwill et al., 1990). However, the required magnitude of differential exhumation necessary to explain the along-strike age variations in northern Labrador over a relatively short latitudinal distance (<150 km) appears to be inconsistent with the very large-wavelength regional updoming.

Alternatively, northward younging of cooling ages might also be attributable to diachronous rift propagation from south to north. Our data indicate that rapid exhumation in the Torngat Mountains started in the latest Jurassic to earliest Cretaceous, which is in good agreement with independent geological evidence for the timing of rift initiation, such as deposition of continental basalts of the Alexis Fm. (139-104 Ma; Umpleby, 1979) and the coarse-clastic syn-rift deposits of the Bjarni Fm. in grabens and half-grabens flanked by Precambrian basement highs along the Labrador Shelf (Figure 5). The Baffin Bay region experienced rift-flank uplift and exhumation during Late Cretaceous rifting, whereas apatite thermochronological data collected in the Sverdrup Basin region (Canada-Greenland Arctic Archipelago) record evidence for Paleogene cooling (Grist and Zentilli, in review). These

observations are consistent with a "zipper'-like northward propagation of rifting and rift-related cooling along the axis of the Labrador Sea from south to north.

Systematic sinusoidal along-strike variations in (U-Th)/He ages seen in both iso-elevation N-S transects appear to be the result of the effect of topographic cooling during relief generation on crustal isotherms. Similar (U-Th)/He age trends at the 450 and 1000 m transects appears to correlate with long wavelength topography (Figures 15 and 17). The wavelengths of the (U-Th)/He age data in both transects (~74 and ~34 km for the 450 and 1000 m transects, respectively) seem to mimic the larger scale topographic wavelength (~79 and ~36 km for the 450 and 1000 m transects, respectively) (Figures 15 and 17). Although apatite (U-Th)/He data from the iso-elevation N-S transects do not directly date fiord incision, they provide important constraints on the timing of relief generation. The data indicate that the long-wavelength relief of the Torngat Mountains was most likely established during the Cretaceous to early Tertiary superimposed on the early Cretaceous rift margin. The data do not provide any temporal constrains on the development of shorter wavelength topography since it is either much younger or not of sufficient amplitude or wavelength to affect shallow crustal isotherms, making it undetectable for the apatite (U-Th)/He thermochronometry. Also worth noticing is that the periodic trend of (U-Th)/He ages appears to mimic the periodicity seen in the topography, suggesting a cross sectional view of the paleotopography through the (U-Th)/He ages indicative of paleodrainages operating orthogonal to the rift margin.

The iso-elevation (U-Th)/He ages imply that the observed high-amplitude relief that developed along the western Labrador continental margin is the result of large-magnitude fluvial erosion and incision during the Late Cretaceous and Early Tertiary; a period that was characterized by a significantly warmer and wetter climate with mean annual temperatures approximately 15 to 27°C warmer than at present at 60°N latitude (Barron, 1983; DeConto et al., 1999). Despite ubiquitous evidence for extensive Pleistocene continental glaciations, Marquette et al. (2004) and Staiger et al. (2005) convincingly demonstrated that glacial erosion had very limited effect on generation of the present day topographic relief in the Torngat Mountains.

Comparison of average post-rift erosional exhumation rates derived from (U-Th)/He and cosmogenic nuclide data shows that long-term erosion rates are significantly faster than short-term Pleistocene estimates for the Torngat Mountains. Apatite (U-Th)/He constraints on average erosion rate estimates since 140 Ma suggest rates <11 m/Myr for the Mt. D'Iberville area and central Torngat Mountains. Erosion rates over the last 20 glacial-interglacial cycles (~10 Ma) obtained from cosmogenic nuclide data from the summits of the Torngat Mountains (<1.5 m/My) (Staiger et al., 2005) suggest that recent erosion rates are slower than the long-term average by a factor of ~7. In addition, estimates of bedrock erosion of ~2.5 m per single glacial cycle at valleys in the Torngat Mountains (Marquette et al., 2004) suggest that probably only ~50 m of relief has been created over 20 glacial cycles since the Miocene due to glacial erosion.

VII. Conclusions

Analysis of apatite (U-Th)/He age data from the Mt. D'Iberville vertical sample profile and numerical forward modeling of the age trend indicate that rapid cooling affecting the Torngat Mountains started at ~140-150 Ma. The thermochronological constraints on the timing of initiation of extension along the western Labrador margin appears to be in excellent agreement with independent geological evidence, such as latest Jurassic and early Cretaceous basaltic volcanism and coarse-clastic syn-rift sedimentation. These data suggest a very protracted rifting history staring as early as ~150 Ma and culminating in the initiation of seafloor spreading in the Labrador Sea and the break-up of the Greenland-Canadian craton at ~65 Ma. This long duration of rifting prior to lithospheric rupture suggests a very protracted or complicated multi-stage history of continental extension that initiated in latest Jurassic times and was followed by long-lived syn-rift sedimentation throughout the Cretaceous.

Apatite (U-Th)/He ages along the E-W transect, collected perpendicular to the Torngat Mountains and the Labrador coast, record differential exhumation and erosion with decreasing magnitude from east to west towards the interior of Ungava Peninsula. Ages near the present-day Labrador coastline are as young as ~78 Ma and are significantly younger than the estimated timing of initial rifting (~140-150 Ma). This observation suggests significant amounts (~1-2 km) of post-rift erosion and incision along the eastern continental margin of the Labrador Sea or renewed rift-related exhumation in late Cretaceous to early Tertiary times. In order to quantify

these processes and evaluate the driving mechanisms explaining these younger ages, samples from offshore boreholes across the extended continental shelf will be necessary.

In the core of the Torngat Mountains, apatite (U-Th)/He ages range from ~200-250 Ma and are roughly consistent with apatite fission track data (~275 Ma) (A. Grist, unpublished data). These ages are considerably older than rifting, define an exhumed partial retention zone (Figure 9), and suggest very limited Mesozoic and Tertiary cooling and exhumation (<1.5 km, from modeled apatite (U-Th)/He ages of the Mt. D'Iberville samples). This conclusion is important since it implies that the rugged and high relief of the Torngat Mountains are not the result of rapid late Tertiary uplift and tectonic processes, but represent an erosional remnant of the uplifted and eroded western continental margin of the Labrador Sea.

West of the Torngat Mountains towards Ungava Bay, apatite (U-Th)/He ages are significantly younger than in the core of Ungava Peninsula (~150-200 Ma). These ages corroborate the nature of the Torngat Mountains as an erosional remnant and suggest substantial post-rift erosion likely related to Mesozoic and Tertiary fluvial erosion and potentially to Pleistocene continental glaciation. Data on erosion rates and sediment discharge of the large river systems (e.g., Korok and Alluviaq rivers) draining the Torngat Mountains to the west into Ungava Bay would be useful for supporting this hypothesis. Additionally, the differential pattern of apatite (U-Th)/He ages observed from the E-W transect closely resembles the age pattern predicted for apatite fission track ages for the pinned divide model of passive margins (Figure 7b)

described by Gallagher et al. (1998) characterized by a significant component of erosion to the west of the Torngat Mountains divide.

Results of transects at 450 m and 1000 m elevation confirm a consistent pattern of increasing apatite (U-Th)/He ages with westward distance away from the Labrador margin. More importantly, both transects show apatite (U-Th)/He ages that appear to mimic the larger scale, coastline-parallel topography of the area, such as major rivers, fiords, and interfluves; a pattern that is consistent with systematic deflection of shallow crustal isotherms during post-rift development of high-amplitude topographic relief. The data only mimics the long wavelength topography (~74 km at 450 m elevation and ~34 km at 1000 m elevation), while smaller scale topographic features have not played a significant role in the disturbance of shallow crustal isotherms. The apparent isotherm deflection as a result of topographic cooling in response to relief generation postdates the onset of latest Jurassic - early Cretaceous rifting and most likely occurred in Cretaceous to early Tertiary times. These data further suggest a limited amount of post-rift erosion and incision with a magnitude of less than 1-2 km. Additional numerical modeling will be required to refine the timing and spatial magnitude of post-rift erosion in more detail.

Figure 1. Photograph showing the rugged topography of the Torngat Mountains of northern Labrador and Quebec, Canada. Highest peaks are >1500 m in elevation. Relief in some areas is greater than 2000 m.

Figure 2. Composite Landsat7 satellite image of Ungava Peninsula and the Torngat Mountains, Labrador and Quebec, Canada. Light blue spectra colors (snow cover) outline high topography in the Torngat Mountains. Drainage divide (light blue dashed line), roughly following the highest Torngat peaks, delineates the Quebec-Labrador provincial boundary. Superimposed structural provinces from west to east: Core Zone (light yellow), Torngat Orogen (clear), and Nain Craton (light purple). KSZ (Komaktorvik Shear Zone), ASZ (Abloviak Shear Zone). Upper right hand inset showing location of study area. Structural provinces modified from ECSOOT geological map (Wardle et al., 2000).

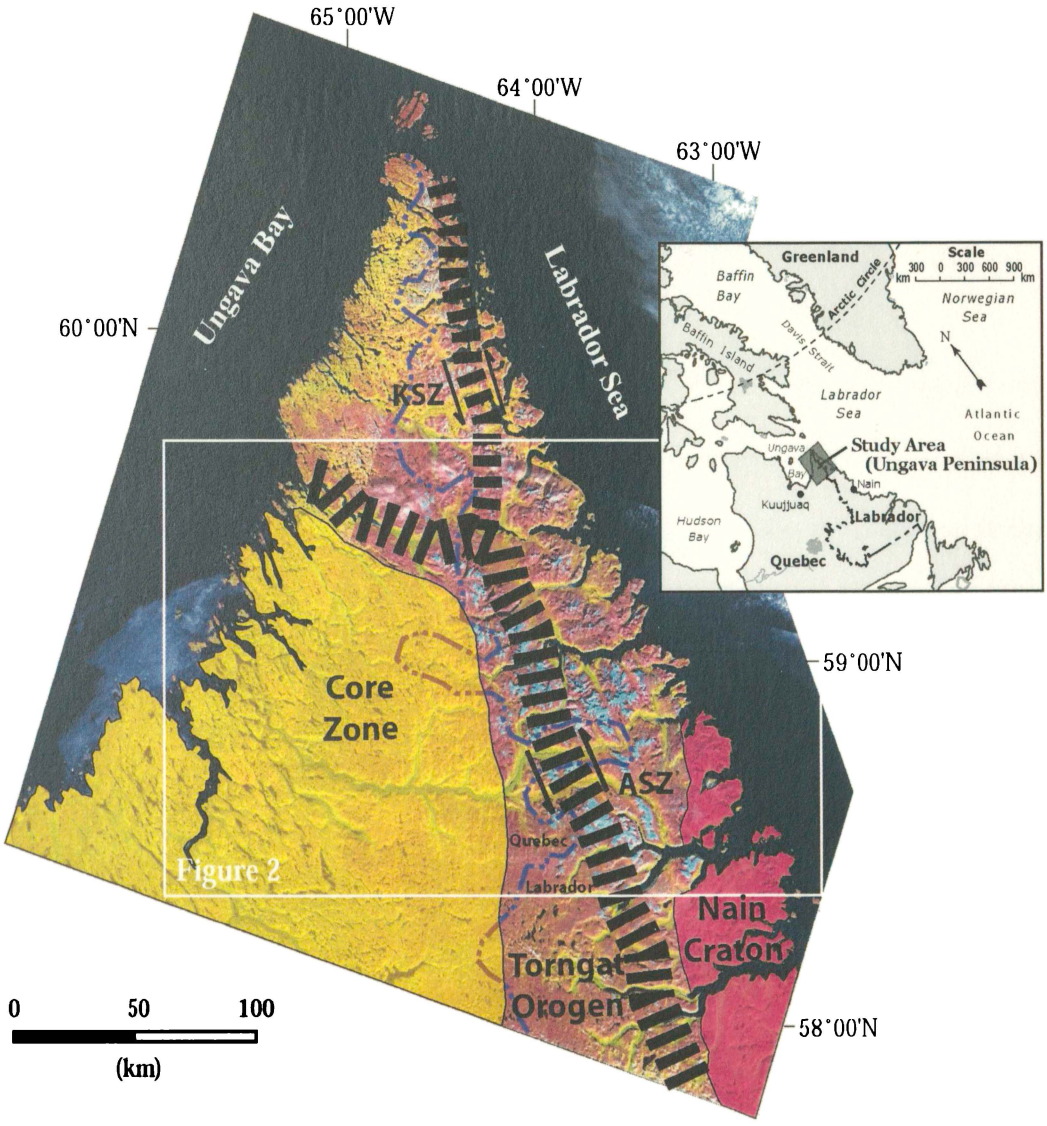
65°00'W
64°00'W
63°00'W
60°00'N
59°00'N
58°00'N
Ungava Bay
Labrador Sea
KSZ
Core Zone
ASZ
Figure 2
Quebec
Labrador
Nain Craton
Torngat Orogen
0
50
100
(km)
Greenland
Baffin Bay
Arctic Circle
Scale
300 0 300 600 900 km
Norwegian Sea
Baffin Island
Davis Strait
N
Labrador Sea
Atlantic Ocean
Ungava Bay
Study Area (Ungava Peninsula)
Nain
Kuujjuaq
Labrador
Hudson Bay
Quebec

Figure 3. Composite Landsat7 satellite image of central Ungava Peninsula and the Torngat Mountains (see Figure 2 for location) showing thermochronological sample locations (open colored circles) and vertical sampling transects (stars) used for this study (see text for details). Major rivers are in blue, main fiords have also been labeled.

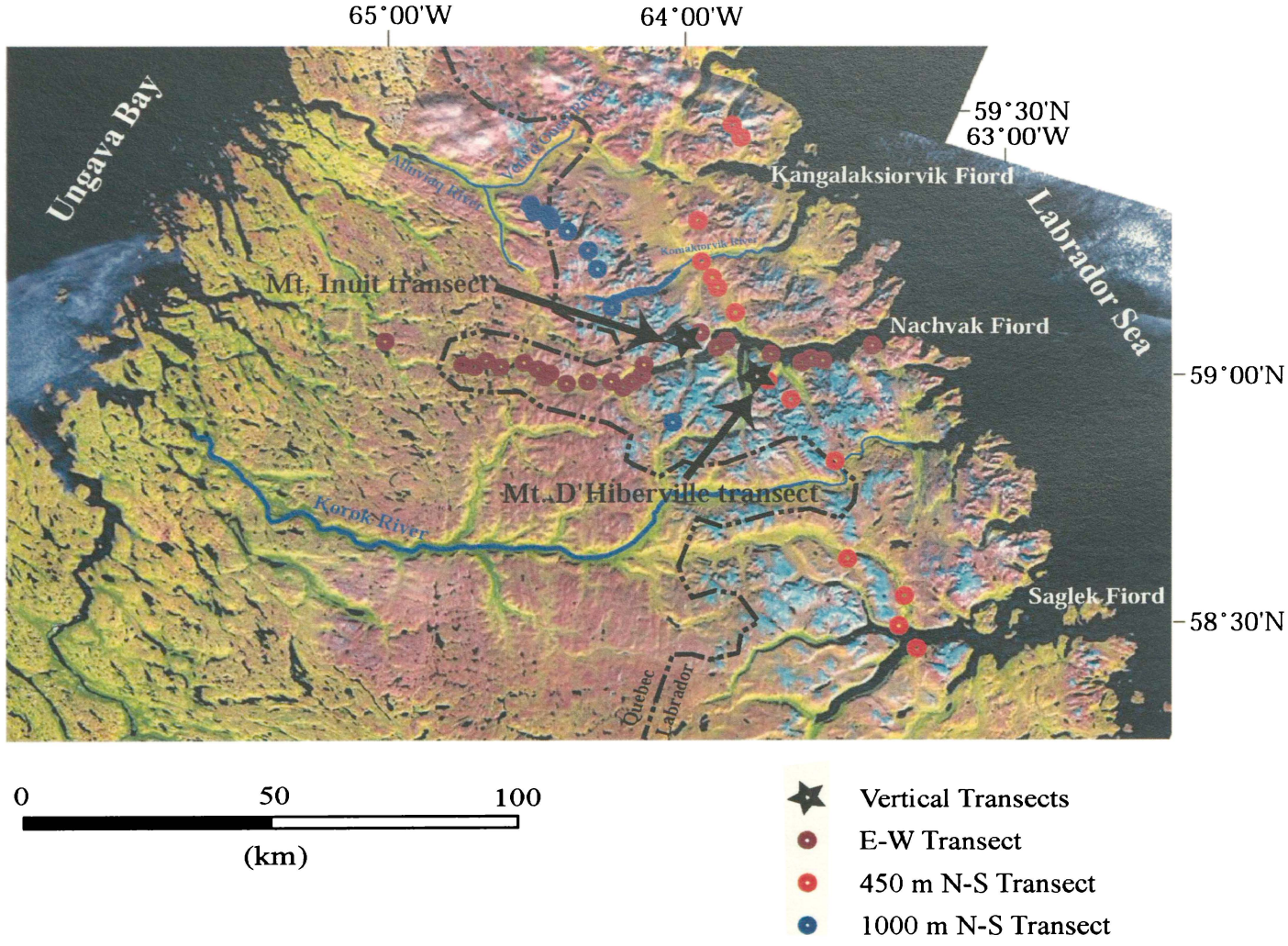
65°00'W
64°00'W
59°30'N
63°00'W
59°00'N
58°30'N
Ungava Bay
Labrador Sea
Kangalaksiorvik Fiord
Nachvak Fiord
Saglek Fiord
Mt. Inuit transect
Mt. D'Iberville transect
Korpk River
Komaktorvik River
Quebec
Labrador
0
50
100
(km)
Vertical Transects
E-W Transect
450 m N-S Transect
1000 m N-S Transect

Figure 4. Geologic map of central Ungava Peninsula showing the location of samples from the two vertical transects, the two N-S transects, and the E-W transect. Geologic map modified after Taylor (1979). Apatite (U-Th)/He ages are labeled next to each individual sample location.

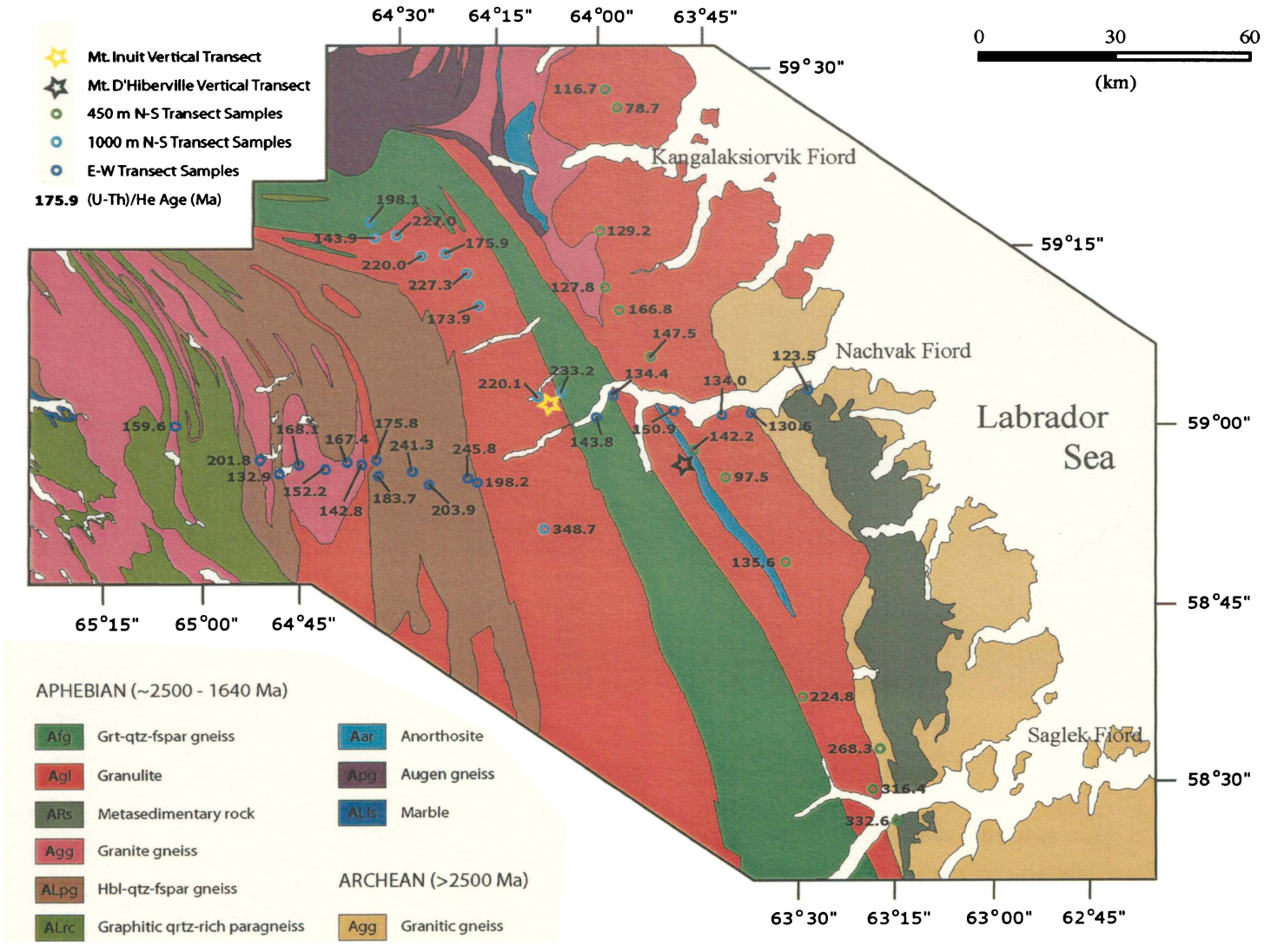
Mt. Inuit Vertical Transect
Mt. D'Hiberville Vertical Transect
450 m N-S Transect Samples
1000 m N-S Transect Samples
E-W Transect Samples
175.9 (U-Th)/He Age (Ma)
0
30
60
(km)
64°30"
64°15"
64°00"
63°45"
59°30"
59°15"
59°00"
58°45"
58°30"
65°15"
65°00"
64°45"
63°30"
63°15"
63°00"
62°45"
Kangalaksiorvik Fiord
Nachvak Fiord
Saglek Fiord
Labrador Sea
116.7
78.7
129.2
127.8
166.8
147.5
123.5
134.4
134.0
130.6
142.2
97.5
135.6
224.8
268.3
316.4
332.6
198.1
227.0
143.9
175.9
220.0
227.3
173.9
220.1
233.2
143.8
150.9
159.6
168.1
167.4
175.8
241.3
245.8
198.2
201.8
132.9
152.2
142.8
183.7
203.9
348.7
APHEBIAN (~2500 - 1640 Ma)
Afg Grt-qtz-fspar gneiss
Agl Granulite
ARs Metasedimentary rock
Agg Granite gneiss
ALpg Hbl-qtz-fspar gneiss
ALrc Graphitic qrtz-rich paragneiss
Aar Anorthosite
Apg Augen gneiss
ALls Marble
ARCHEAN (>2500 Ma)
Agg Granitic gneiss

Figure 5. Geological cross-section through Saglek Bank, Labrador Shelf, based on interpretation of regional seismic profiles. Note landward (westward) dipping normal faults in Precambrian basement formed during the Early Cretaceous rifting of the Canadian-Greenland craton. Modified after Balkwill et al. (1990).

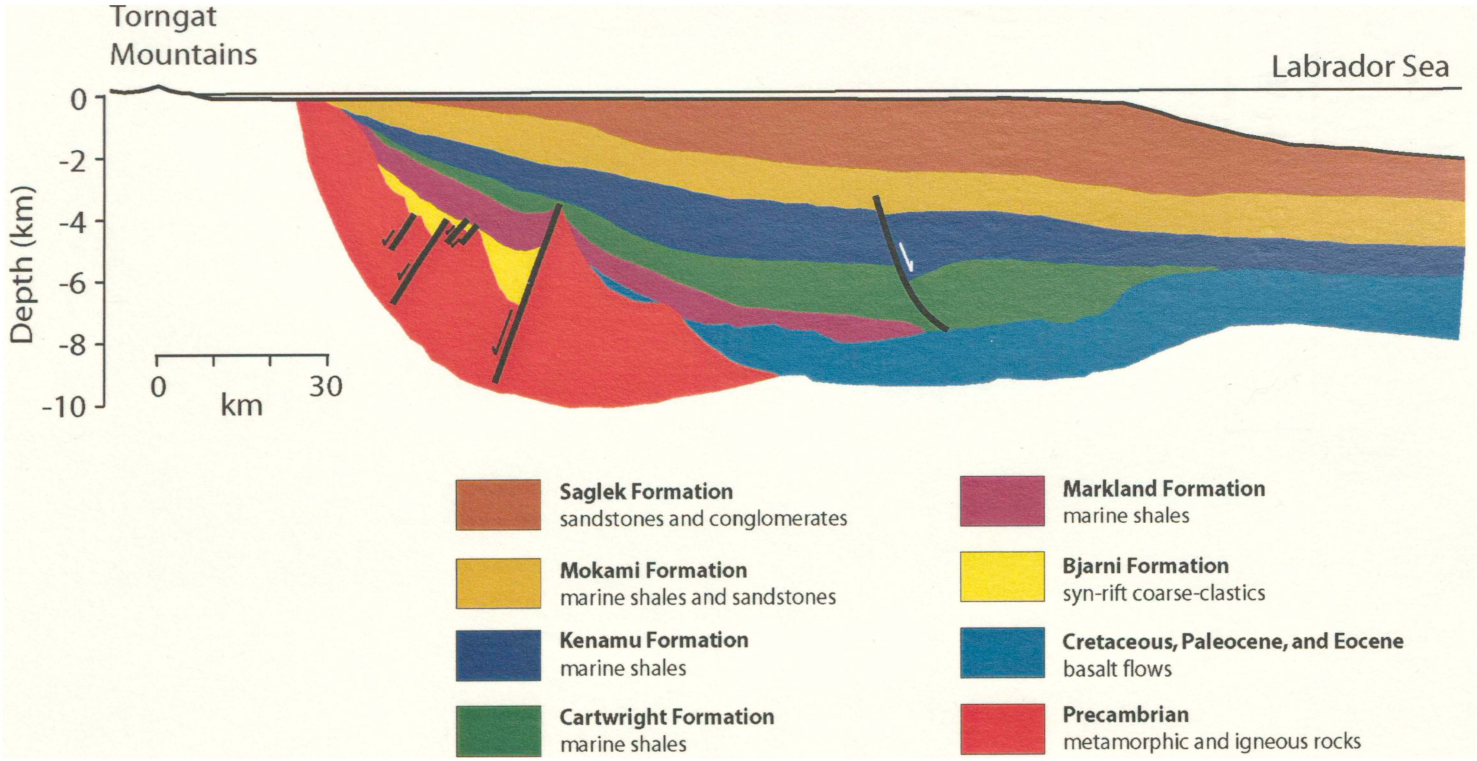
Torngat
Mountains
Labrador Sea
Depth (km)
0
-2
-4
-6
-8
-10
0
30
km
Saglek Formation
sandstones and conglomerates
Markland Formation
marine shales
Mokami Formation
marine shales and sandstones
Bjarni Formation
syn-rift coarse-clastics
Kenamu Formation
marine shales
Cretaceous, Paleocene, and Eocene
basalt flows
Cartwright Formation
marine shales
Precambrian
metamorphic and igneous rocks

Figure 6. Topographic profile across Ungava Peninsula and the Torngat Mountains contrasting the low relief (<500 m), low elevation (<700 m) topography of the western side of the peninsula with the much higher relief (>1500 m), high elevation topography (>1500 m) of the eastern side of the peninsula. Modified after J. Gosse (unpublished data).

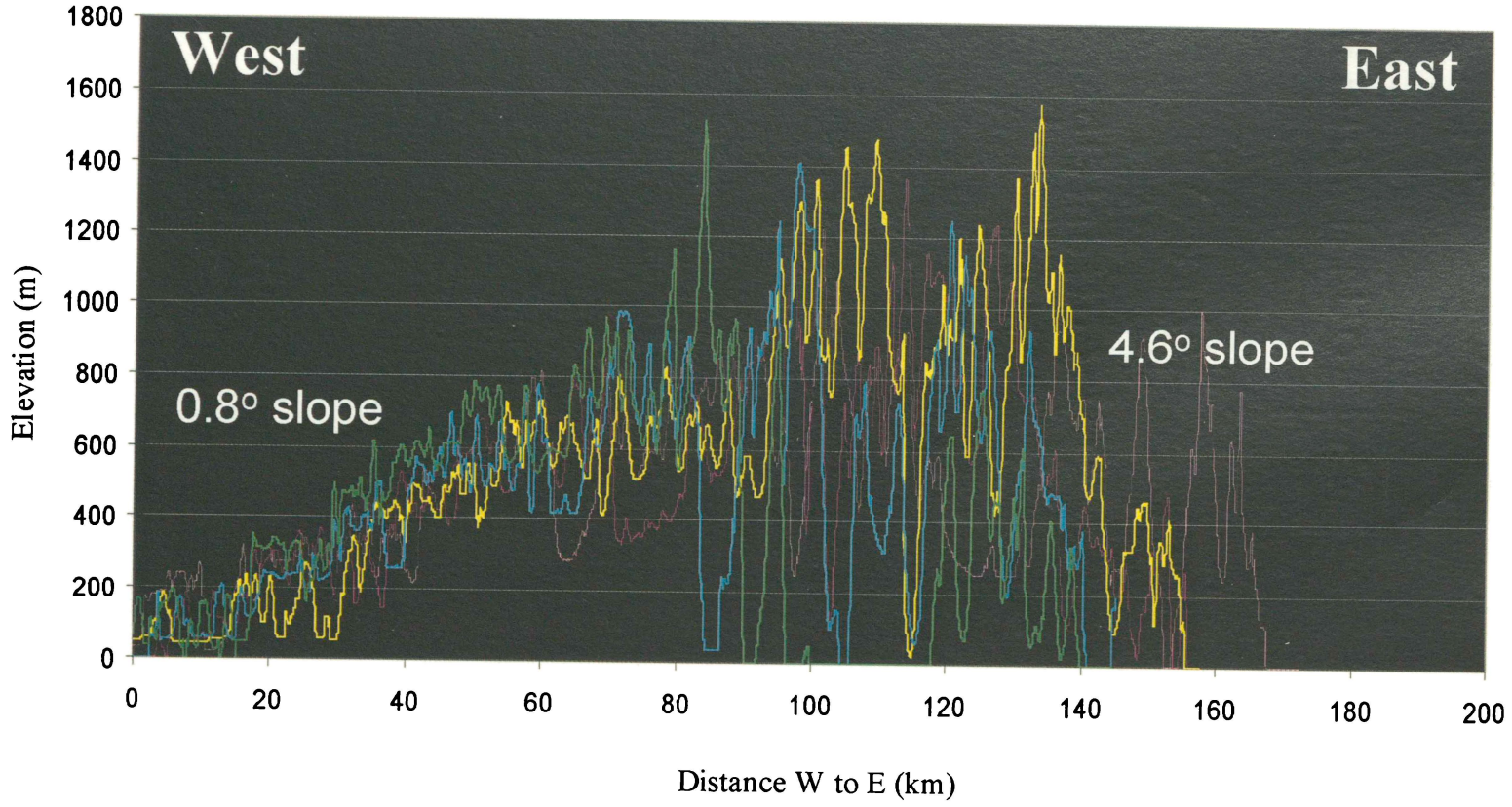
West
East
0.8° slope
4.6° slope
Elevation (m)
1800
1600
1400
1200
1000
800
600
400
200
0
0
20
40
60
80
100
120
140
160
180
200
Distance W to E (km)

Figure 7. Conceptual models for the evolution of passive margins and their predicted spatial trend in apatite thermochronological data. Figure 7(a) is the scarp retreat model and Figure 7(b) is the pinned divide model, both described in the text. Vertical arrow in Figures (a) and (b) represents the original height of the escarpment. Dashed topographic lines indicate the type of escarpment erosion: retreat for (a) and down-wearing for (b). The bottom figure illustrates the pattern of thermochronological data - in this figure, apatite fission track (FT) data - observed in a direction perpendicular to the escarpment. **(A)** represents the location of the coastal plain; **(B)** the location of the scarp edge; and **(C)** the location inland of the escarpment. Modified after Gallagher et al. (1998).

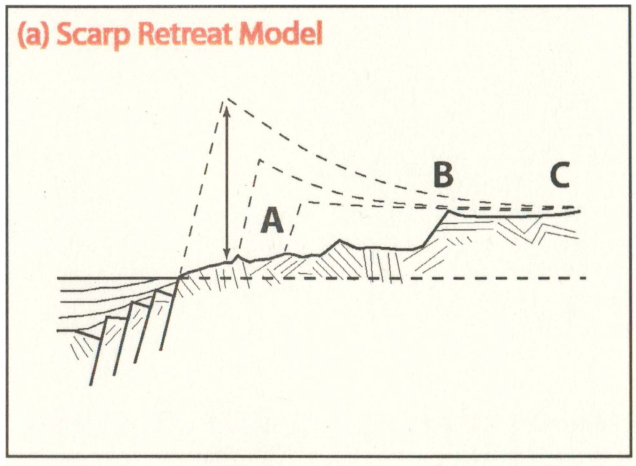
(a) Scarp Retreat Model
A
B
C

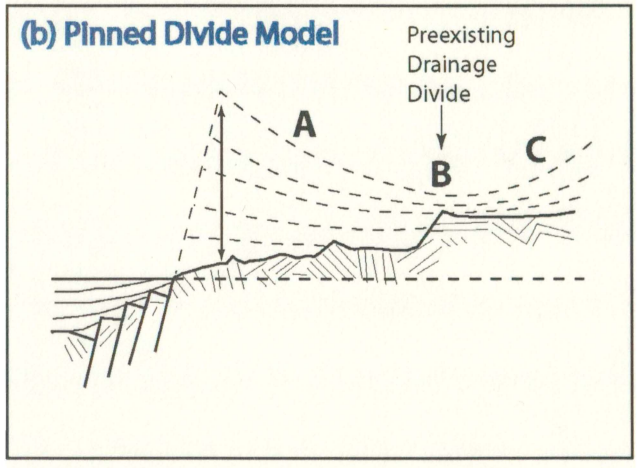
(b) Pinned Divide Model
Preexisting
Drainage
Divide
A
B
C

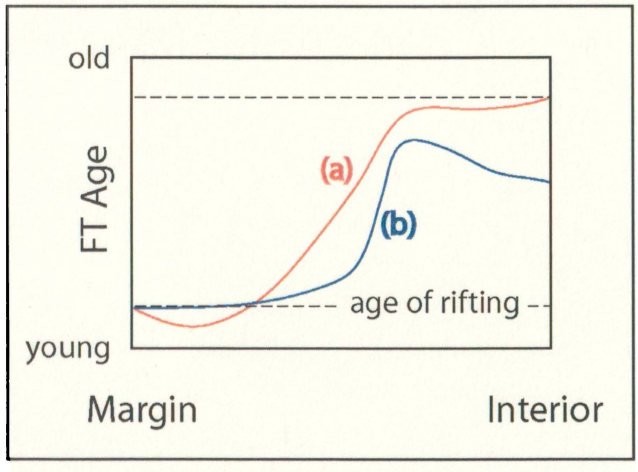
old
FT Age
young
(a)
(b)
age of rifting
Margin
Interior

Figure 8. Pattern of apatite (U-Th)/He ages (rectangles) with distance away from the Labrador Coast along the E-W transect. Only samples between sea level and 560 m have been included. Mean topographic elevation along E-W transect in gray. A best fit line through the data illustrates the parabolic pattern of apatite (U-Th)/He ages and a flattening trend towards the eastern end (see Figure 9). Yellow area attempts to highlight the maximum and minimum age values of the data that follows the general E-W parabolic trend of the ages. All error bars are 2-sigma. Samples with horizontal error bars have been extrapolated from other transects and are also <560 m in elevation. See Figures 3 and 4 for transect location.

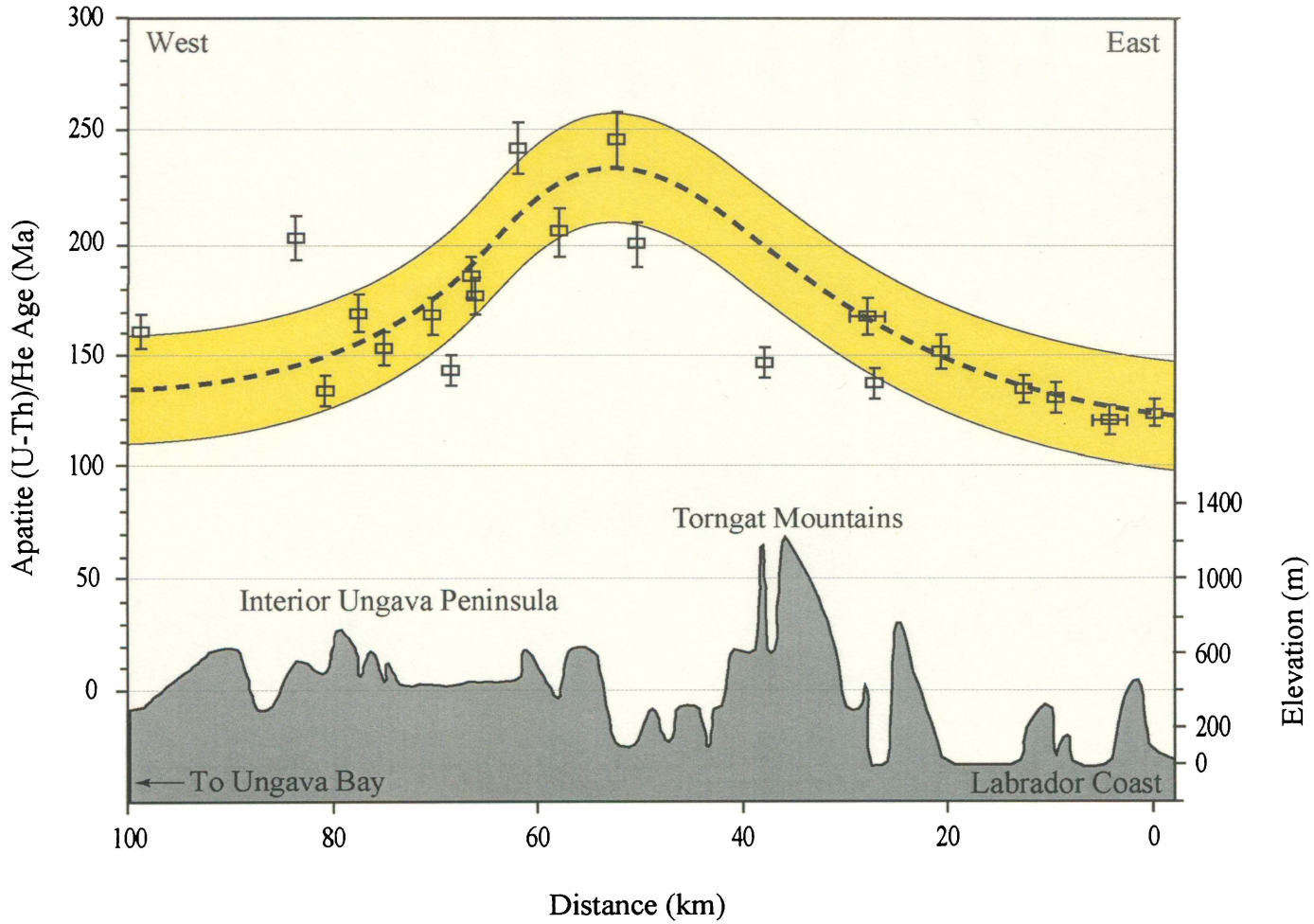
West
East
Apatite (U-Th)/He Age (Ma)
300
250
200
150
100
50
0
Torngat Mountains
Interior Ungava Peninsula
To Ungava Bay
Labrador Coast
1400
1000
600
200
0
Elevation (m)
100
80
60
40
20
0
Distance (km)

Figure 9. E-W transect from Figure 8 showing large red striped areas highlighting the three different clusters of data used to approximate the shape and curvature for a best fit line. Out in the Labrador Sea, the deposition of the Alexis and Bjarni Formations are the first clues for rifting in the area. Their depositional ages are probably associated with rapid uplift of the Labrador coast which would produce invariant apatite (U-Th)/He ages at the bottom of an exhumed apatite HePRZ. Apatite (U-Th)/He ages at the eastern end of the transect become invariant due to westward tilting of the Labrador continental margin. Younger apatite (U-Th)/He ages west from the core of the Torngat Mountains could be explained by Mesozoic to Tertiary fluvial erosion and potentially to Pleistocene continental glaciation. Apatite (U-Th)/He ages younger than Mt. D'Iberville at the coast could also be explained by significant amounts of post-rift erosion and incision.

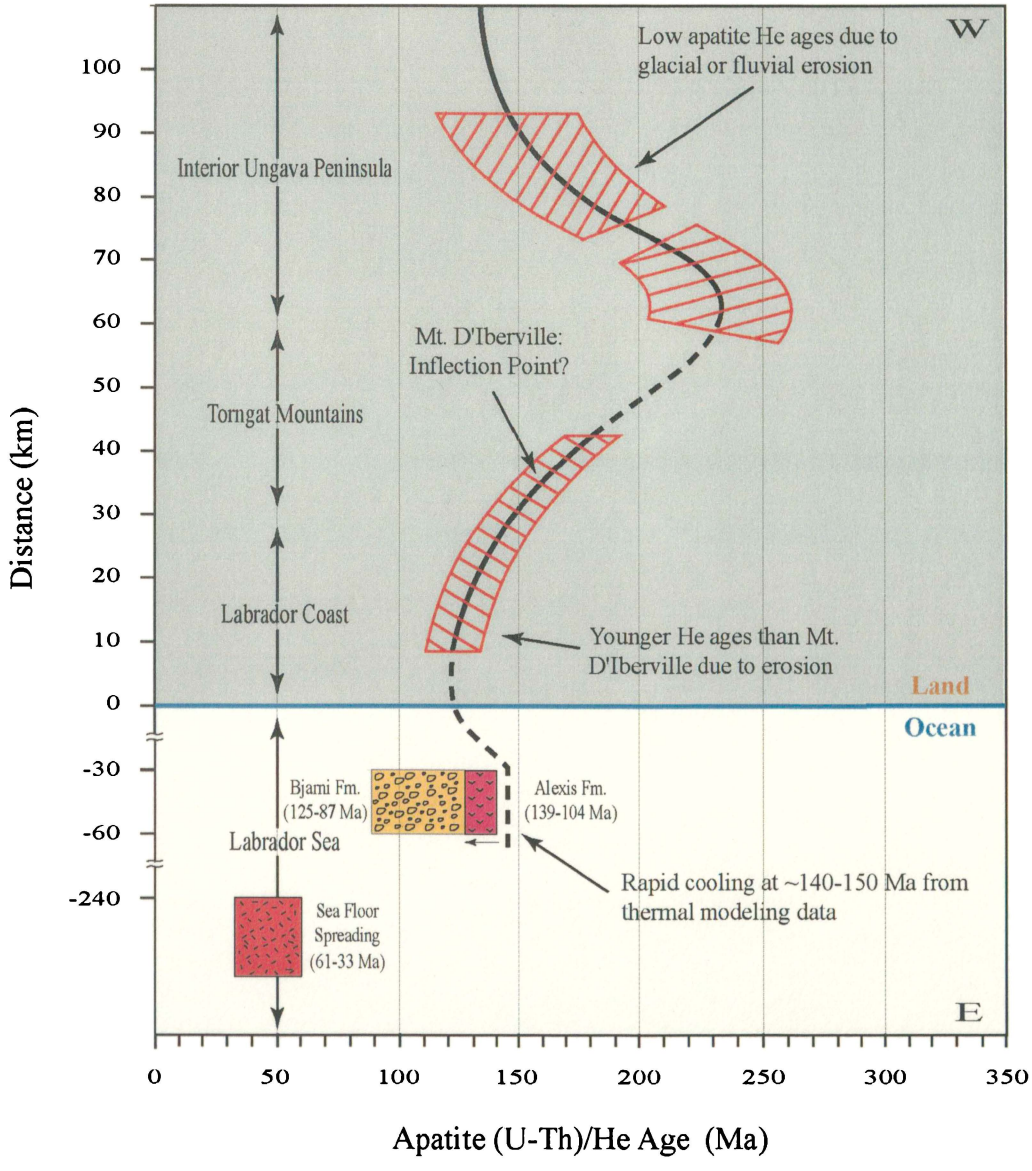
W
Low apatite He ages due to glacial or fluvial erosion
Interior Ungava Peninsula
Mt. D'Iberville: Inflection Point?
Torngat Mountains
Labrador Coast
Younger He ages than Mt. D'Iberville due to erosion
Land
Ocean
Bjami Fm. (125-87 Ma)
Alexis Fm. (139-104 Ma)
Labrador Sea
Rapid cooling at ~140-150 Ma from thermal modeling data
Sea Floor Spreading (61-33 Ma)
E
Distance (km)
100
90
80
70
60
50
40
30
20
10
0
-30
-60
-240
0
50
100
150
200
250
300
350
Apatite (U-Th)/He Age (Ma)

Figure 10. Mount D'Iberville vertical sample profile showing a decrease in apatite (U-Th)/He ages with decreasing elevation. A best fit line through the data (dashed line) shows a positive linear function. All errors are 2-sigma.

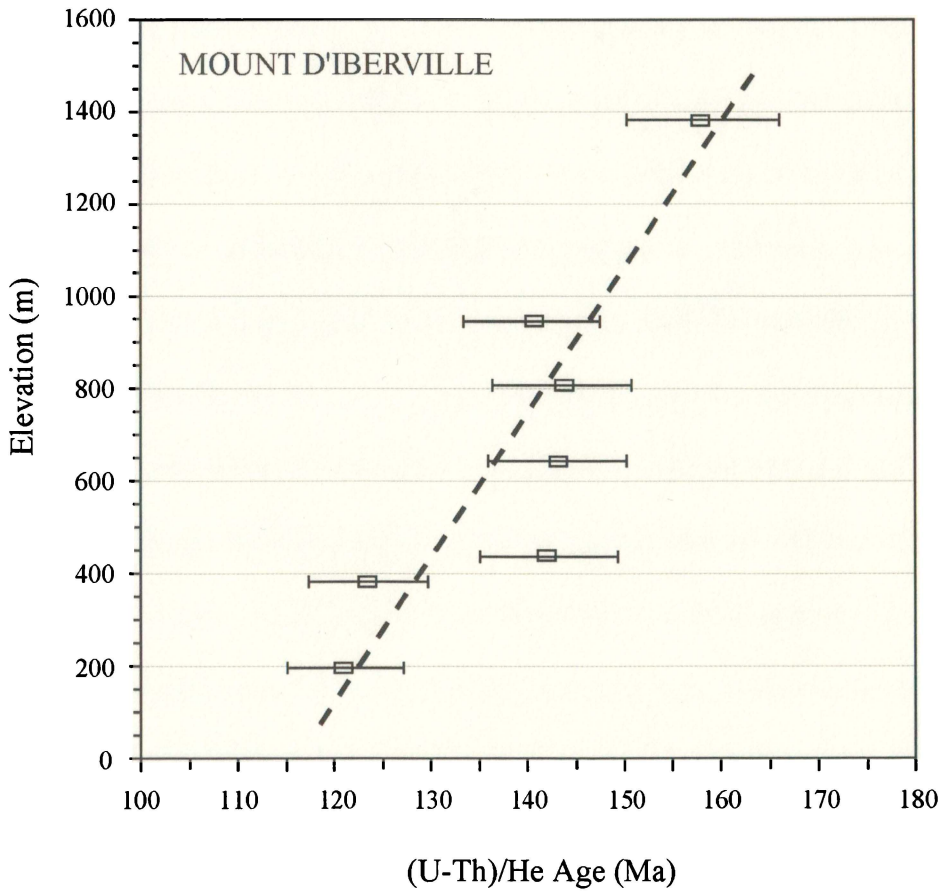
MOUNT D'IBERVILLE
Elevation (m)
1600
1400
1200
1000
800
600
400
200
0
100
110
120
130
140
150
160
170
180
(U-Th)/He Age (Ma)

Figure 11. Diagram showing observed apatite (U-Th)/He age data from Mount D'Iberville vertical transect (see Table 1) plotted against paleo-temperature difference from structurally highest sample. Paleo-temperature difference is estimated based on elevation difference, assuming a geothermal gradient of 25°C/km (see text about geothermal gradient assumption) and no significant post-rift crustal tilting. Curves (1-6) represent predicted vertical transect age patterns derived from forward modeling of specific temperature-time histories shown in Figure 12. Model runs 1-3 yield modeled age patterns that are too young for the lower half of the Mt. D'Iberville transect indicative of overestimating post-rift cooling/erosion. Model runs 4-6 yield results that are in good agreement with the observed age-elevation pattern and are indicative of rapid rift-related cooling during the latest Jurassic to Early Cretaceous and limited post-rift cooling/erosion.

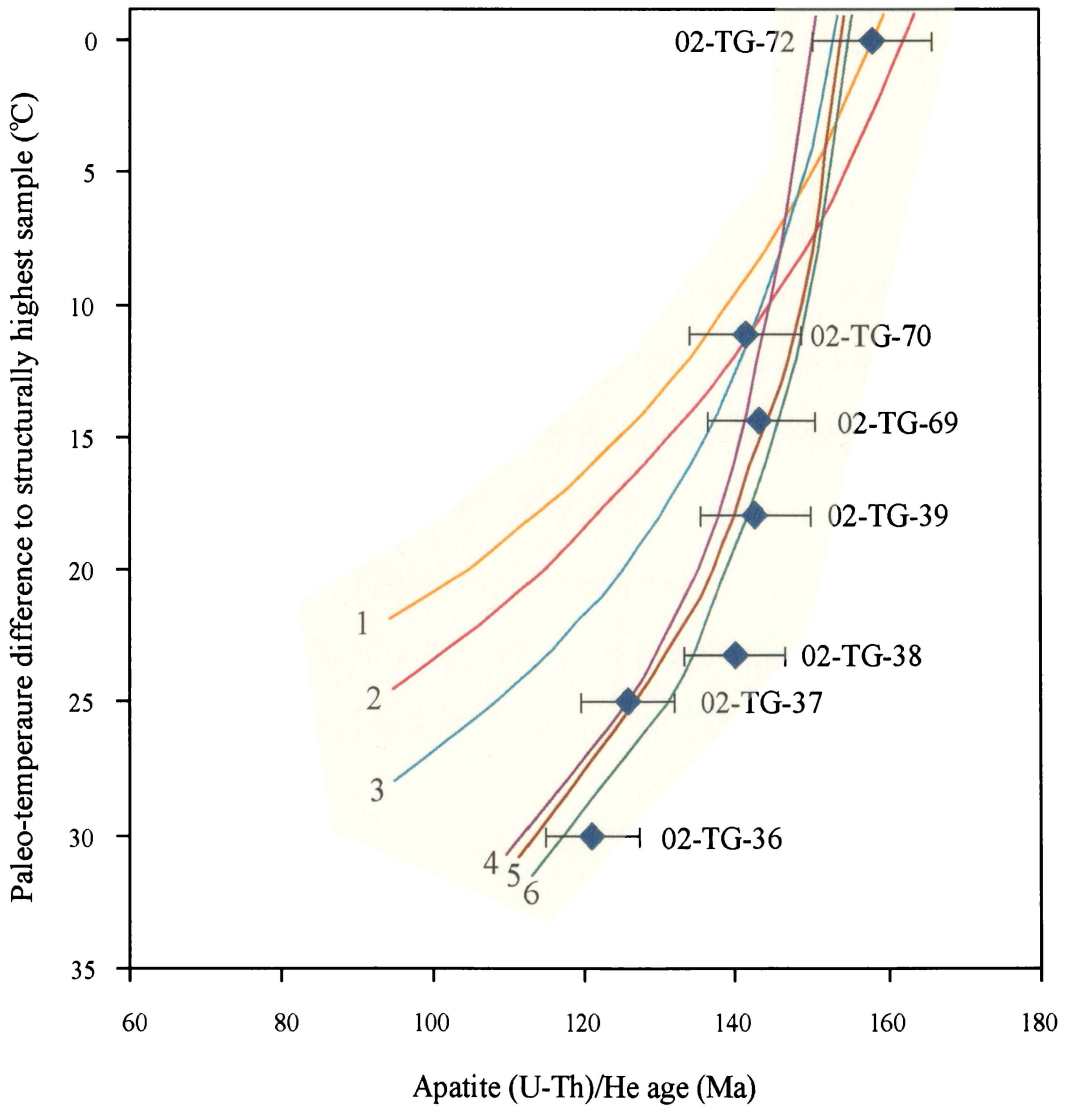
Paleo-temperaure difference to structurally highest sample (°C)
0
5
10
15
20
25
30
35
60
80
100
120
140
160
180
Apatite (U-Th)/He age (Ma)
02-TG-72
02-TG-70
02-TG-69
02-TG-39
02-TG-38
02-TG-37
02-TG-36
1
2
3
4
5
6

Figure 12. Temperature-time paths used for forward modeling of Mount D'Iberville (U-Th)/He vertical transect age data (see Figure 11). Temperature-time paths are only those of structurally highest sample (02-TG-72), while structurally deeper samples were modeled with a constant temperature offset. Apatite (U-Th)/He thermochronometry data are insensitive to temperatures >80°C, but thermal evolution (>80°C) is estimated based on older apatite (U-Th)/He ages from the core of the Torngat Mountains and apatite fission track data (A. Grist, unpublished data).

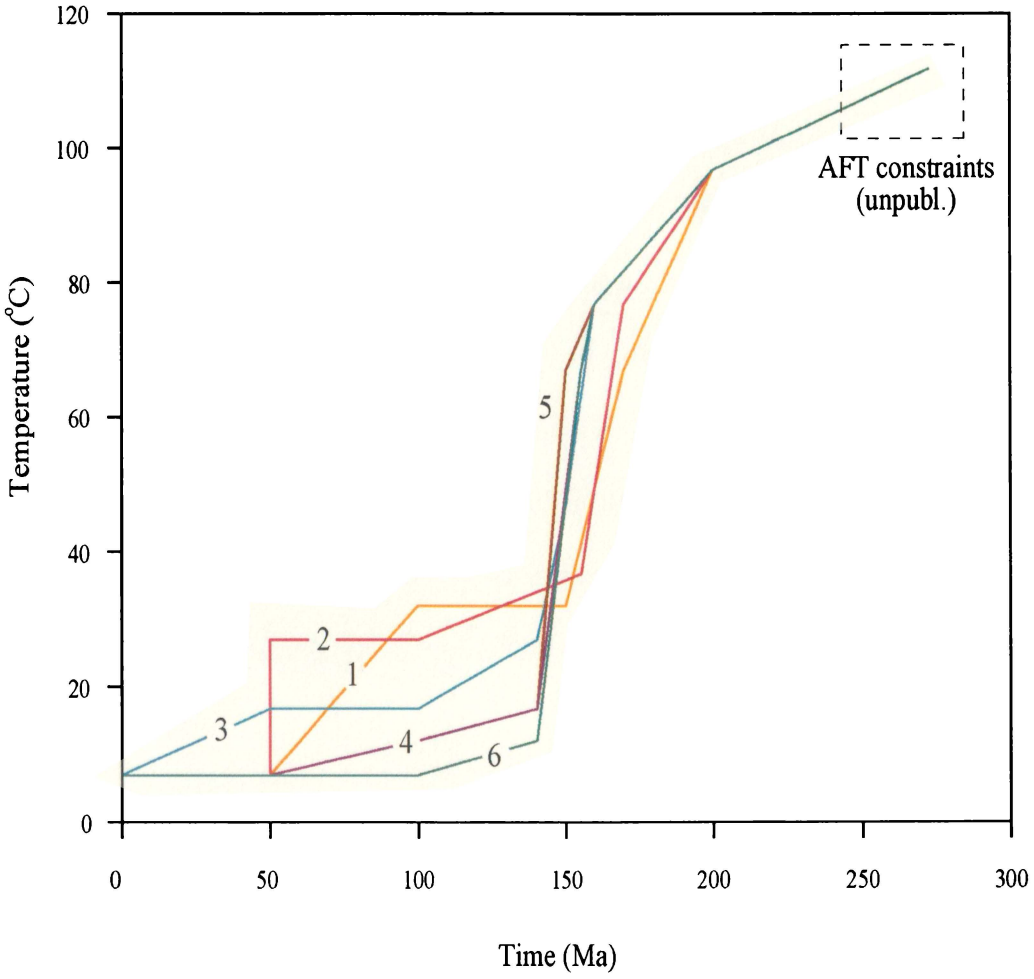
120
100
80
60
40
20
0
Temperature (°C)
0
50
100
150
200
250
300
Time (Ma)
AFT constraints
(unpubl.)
1
2
3
4
5
6

Figure 13. Best-fit temperature-time paths for all samples from the Mount D'Iberville vertical apatite (U-Th)/He transect (model run 5 in Figures 11 and 12). Results indicate that the entire transect underwent rapid cooling from >80°C to <40°C between ~150-140 Ma. Final erosional exhumation and cooling to mean annual surface temperature are unconstrained by forward modeling, but is limited to <35°C for the structurally deepest sample and <5°C for the structurally highest sample since ~140 Ma. All temperature-time paths converge at ~5°C, the modern annual surface temperature. AHe PRZ: Apatite Helium Partial Retention Zone.

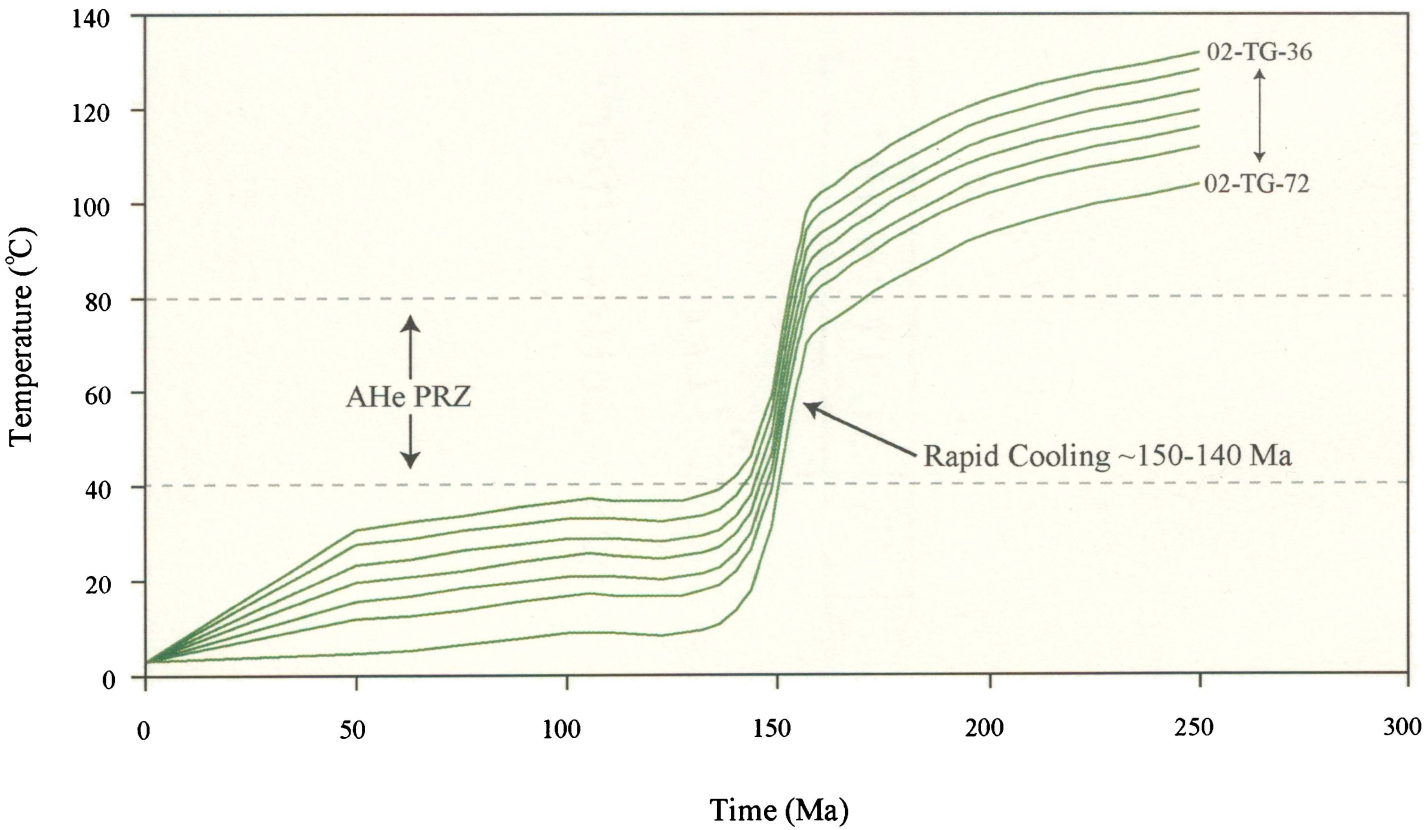
140
120
100
80
60
40
20
0
Temperature (°C)
0
50
100
150
200
250
300
Time (Ma)
02-TG-36
02-TG-72
AHe PRZ
Rapid Cooling ~150-140 Ma

Figure 14. N-S transect collected at a constant elevation of ~450 m. Illustrated are topography (gray) and apatite (U-Th)/He ages (rectangles). Best fit yellow band shows the trend in apatite (U-Th)/He ages. Error bars are 2-sigma. KF: Kangalaksiorvik Fiord; KMR: Komaktorvik River; NF: Nachvak Fiord; KR: Korok River; SF: Saglek Fiord.

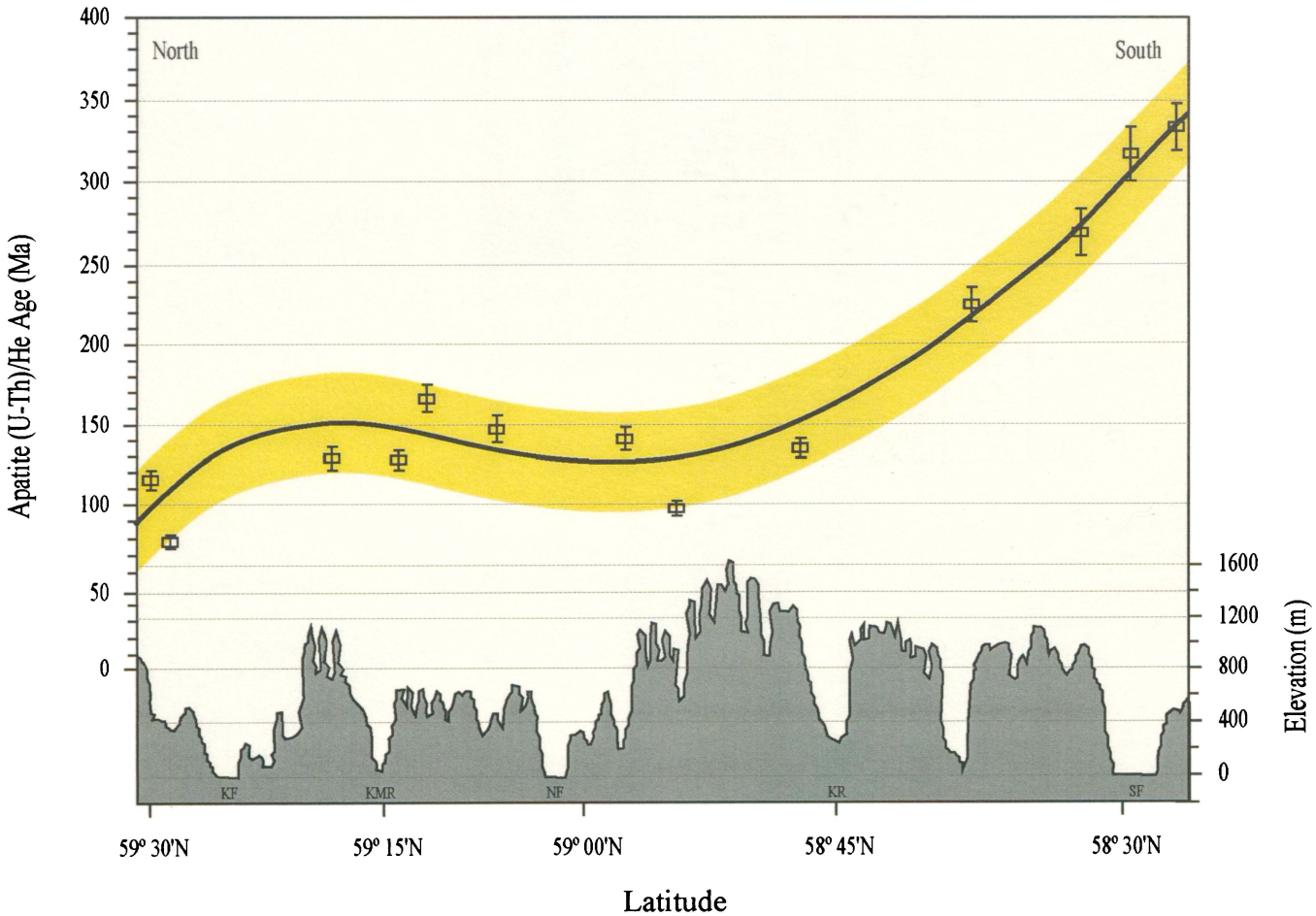
North
South
Apatite (U-Th)/He Age (Ma)
400
350
300
250
200
150
100
50
0
1600
1200
800
400
0
Elevation (m)
KF
KMR
NF
KR
SF
59° 30'N
59° 15'N
59° 00'N
58° 45'N
58° 30'N
Latitude

Figure 15. ~450 m N-S transect interpretation diagram. Topography (gray) from Figure 14 and selected apatite (U-Th)/He ages (rectangles) from the Nachvak Fiord area. Heavy and light curves are apatite (U-Th)/He age trend and uncertainty envelopes, respectively. Curves are dashed away from the Nachvak area samples. Shown are the wavelengths of major topographic features and the half wavelength of the apatite (U-Th)/He age trend. Error bars are 2-sigma. KF: Kangalaksiorvik Fiord; KMR: Komaktorvik River; NF: Nachvak Fiord; KR: Korok River; SF: Saglek Fiord.

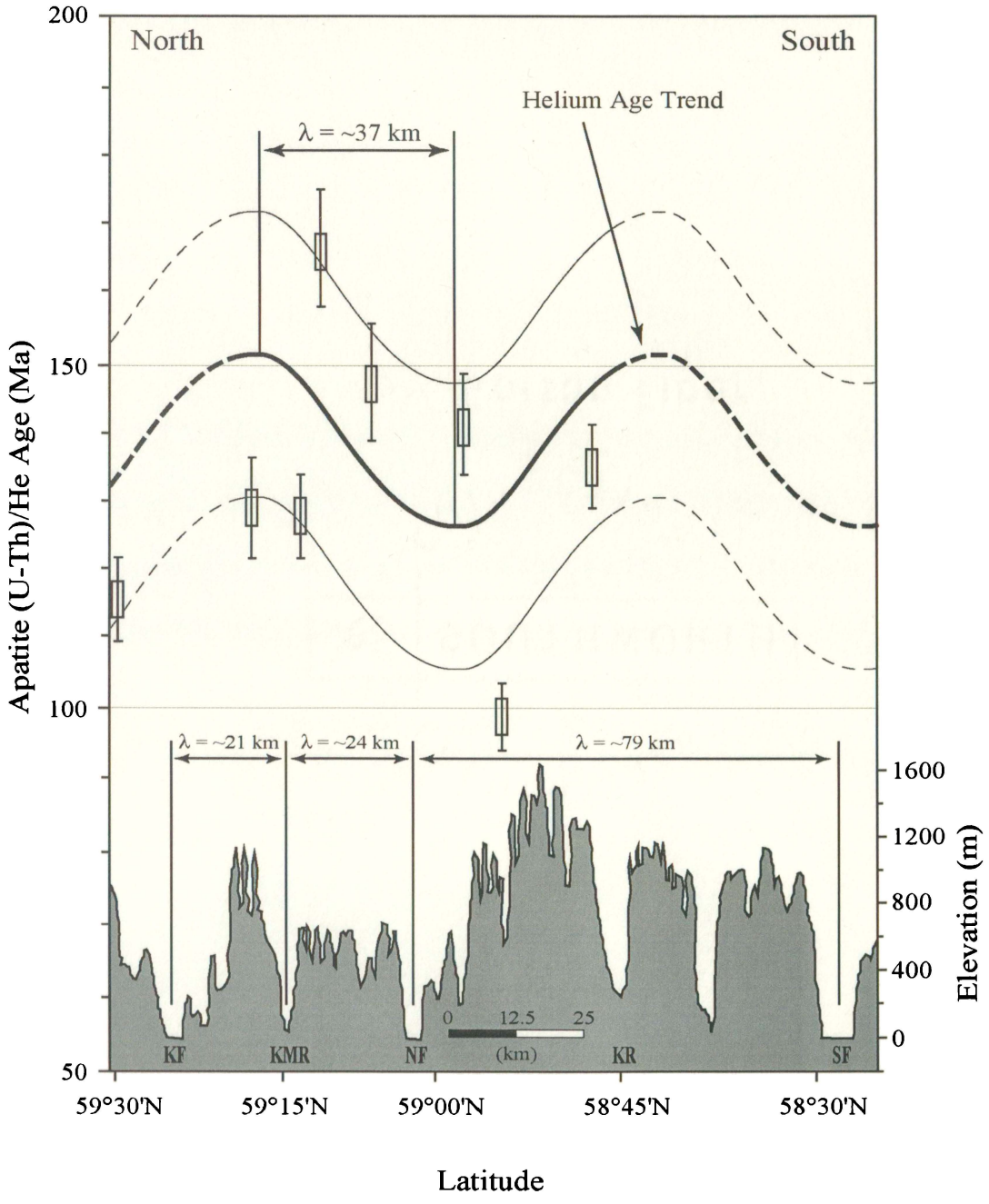
North
South
Helium Age Trend
λ = ~37 km
λ = ~21 km
λ = ~24 km
λ = ~79 km
200
150
100
50
Apatite (U-Th)/He Age (Ma)
1600
1200
800
400
0
Elevation (m)
0
12.5
25
(km)
KF
KMR
NF
KR
SF
59°30'N
59°15'N
59°00'N
58°45'N
58°30'N
Latitude

Figure 16. N-S transect collected at a constant elevation of ~1000 m. Illustrated are topography (gray) and apatite (U-Th)/He ages (rectangles). Yellow band used to show a near-horizontal linear fit through the data with significant random scatter about the mean at ~200 Ma. Error bars are 2-sigma. KL: Komaktorvik Lakes; NL: Nachvak Lake.

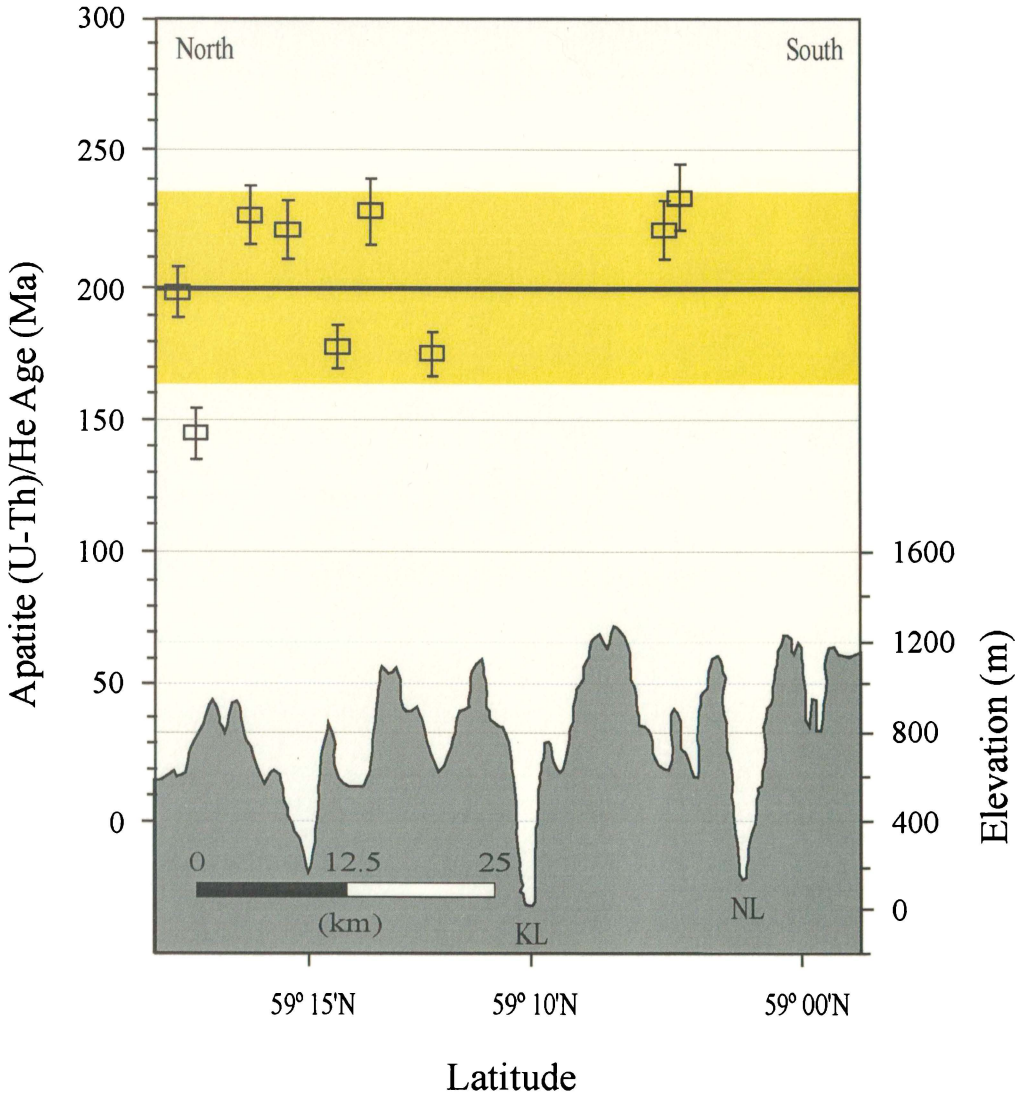
North
South
300
250
200
150
100
50
0
Apatite (U-Th)/He Age (Ma)
1600
1200
800
400
0
Elevation (m)
0
12.5
25
(km)
KL
NL
59° 15'N
59° 10'N
59° 00'N
Latitude

Figure 17. ~1000 m N-S transect interpretation diagram. Topography (gray) from Figure 16 and selected apatite (U-Th)/He ages (rectangles) from area north of Nachvak Lake. Heavy and light curves are apatite (U-Th)/He age trend and uncertainty envelopes, respectively. Curves are dashed where there is no sample control. Shown are the wavelengths of major topographic features and the half wavelength of the apatite (U-Th)/He age trend. Error bars are 2-sigma. KL: Komaktorvik Lakes; NL: Nachvak Lake.

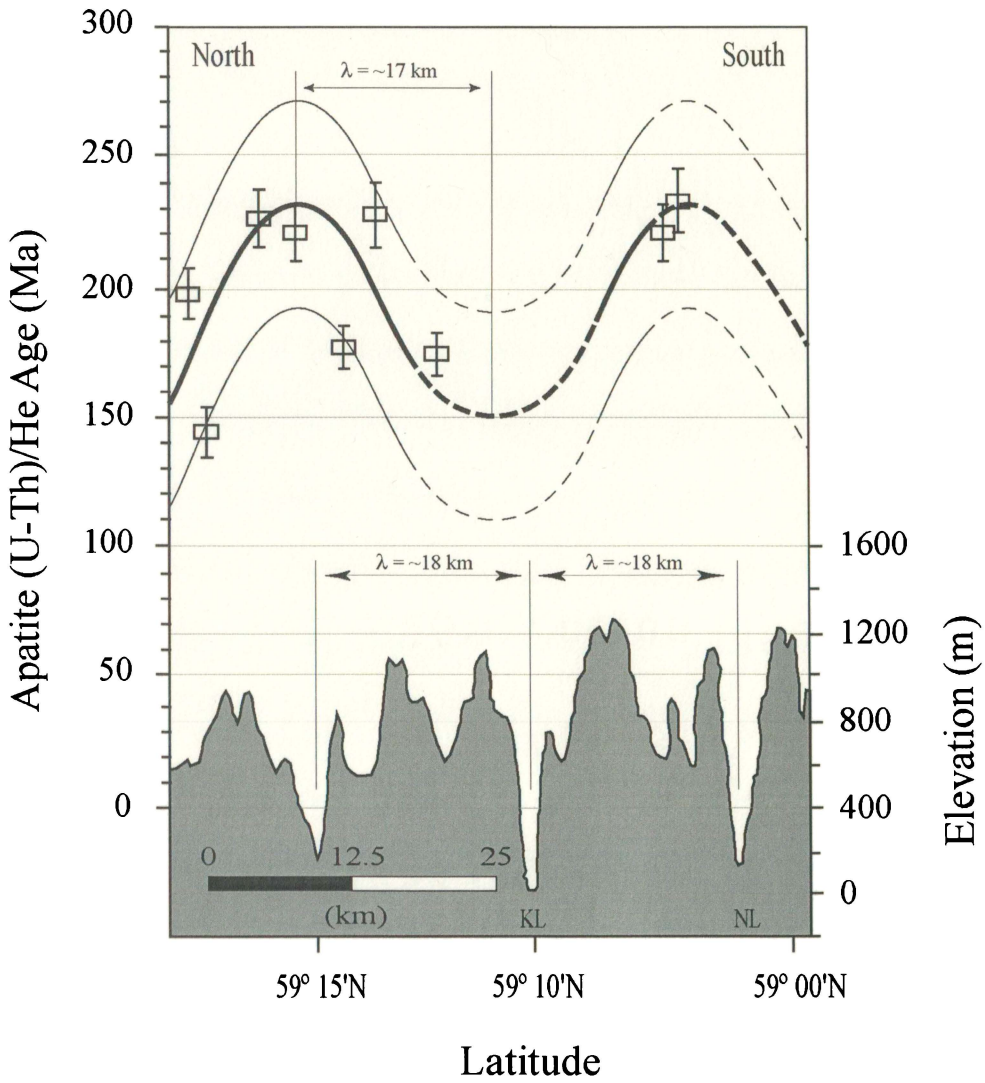
North
South
λ = ~17 km
λ = ~18 km
λ = ~18 km
Apatite (U-Th)/He Age (Ma)
300
250
200
150
100
50
0
1600
1200
800
400
0
Elevation (m)
0
12.5
25
(km)
KL
NL
59° 15'N
59° 10'N
59° 00'N
Latitude

Figure 18. Power spectral analysis of one-dimensional topography along the 1000 m transect calculated using a forward Fast Fourier Transform. The power spectrum is defined as the square of the linear spectrum magnitude and indicates the power of each frequency component. The resulting power spectra are dimensionless in the vertical direction. Frequency (1/pixel) is then converted to wavelength λ (km). Analysis of the one-dimensional topography along the 1000 m transect shows significant topographic wavelengths of ~31, ~25, ~20, and ~10 km; with the ~31 and ~10 km topographic signals representing the two dominant wavelengths. In logarithmic space, the power appears to approximate a straight line, which indicates that the topography displays fractal properties, meaning the topography is scale-invariant.

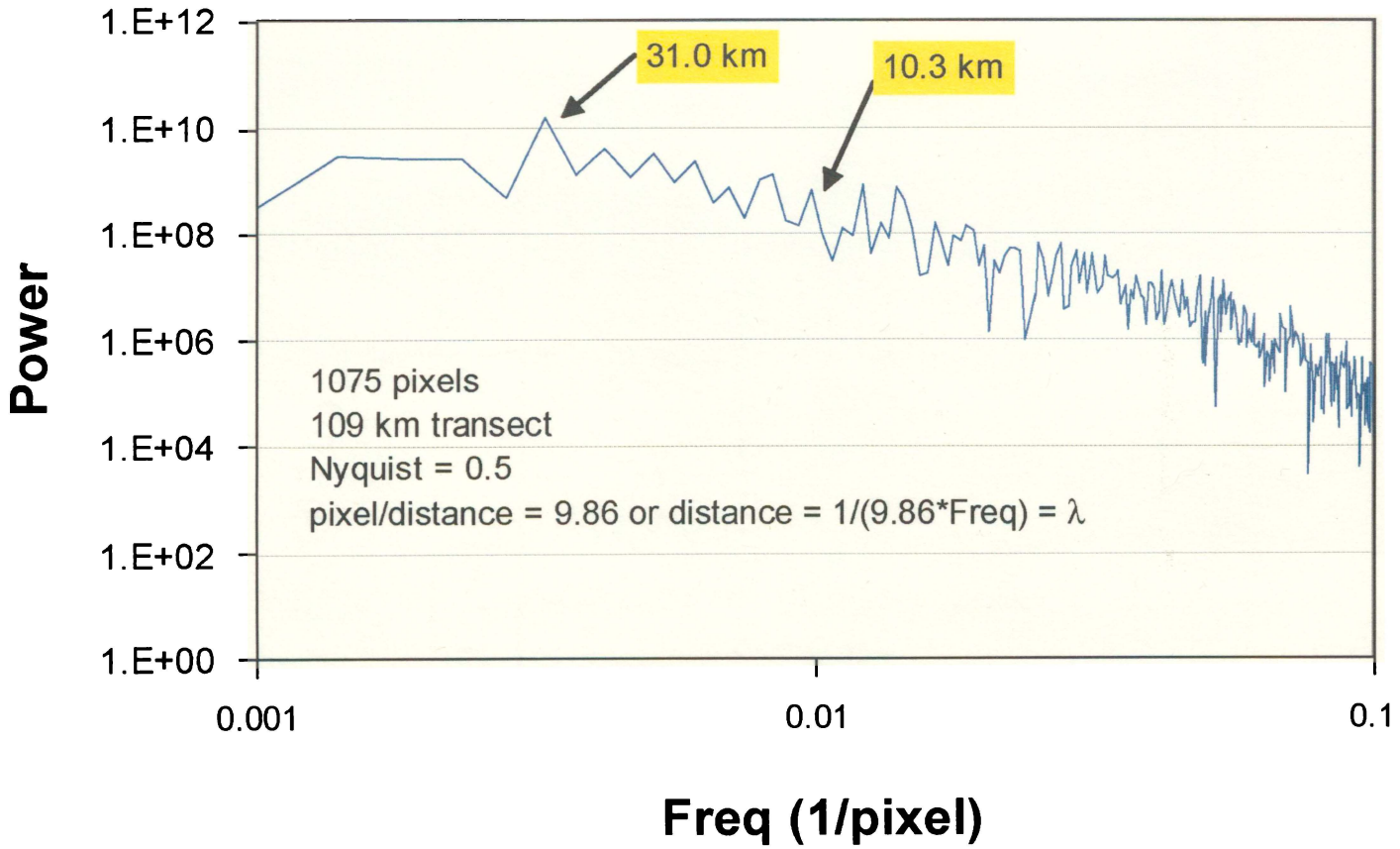
1.E+12
1.E+10
1.E+08
1.E+06
1.E+04
1.E+02
1.E+00
Power
31.0 km
10.3 km
1075 pixels
109 km transect
Nyquist = 0.5
pixel/distance = 9.86 or distance = 1/(9.86*Freq) = λ
0.001
0.01
0.1
Freq (1/pixel)

Table 1. Summary of apatite (U-Th)/He age data from the Torngat Mountains, northern Labrador and Quebec, Canada.

Sample	Latitude, North	Longitude, West	Elevation, m	He, ncc	U, ppm	Th, ppm	Correction factor, Ft	Corrected age (Ma) ± 2σ	Rock Type
E-W Transect									
02-TG-01	N58°59'27.2"	W064°43'47.5"	463	0.26	2.89	3.75	0.71	168.1± 8.6	Granite gneiss
02-TG-02	N58°58'07.5"	W064°32'58.2"	446	2.24	18.46	50.38	0.67	183.7 ± 14.6	Paragneiss
02-TG-03	N58°58'06.7"	W064°33'04.9"	438	4.93	11.16	1.54	0.80	175.8 ± 8.8	Paragneiss
02-TG-04	N58°58'37.4"	W064°34'16.4"	418	0.84	11.14	0.83	0.67	142.8 ± 10.8	Granulite
02-TG-05	N58°58'47.9"	W064°36'37.5"	428	1.52	6.41	12.51	0.74	167.4 ± 4.7	Granite gneiss
02-TG-06	N58°58'28.3"	W064°40'40.3"	437	0.73	3.51	4.47	0.73	152.2 ± 26.2	Granite gneiss
02-TG-07	N58°57'48.2"	W064°46'48.9"	490	1.13	8.50	3.33	0.71	132.9 ± 12.6	Granite gneiss
02-TG-08	N58°58'03.4"	W064°49'24.9"	552	19.82	43.21	6.90	0.81	201.8 ± 11.7	Granite gneiss
02-TG-12	N59°01'20.2"	W065°03'54.3"	301	4.81	14.62	6.13	0.76	159.6 ± 2.5	Granite gneiss
02-TG-14	N58°56'52.4"	W064°28'29.6"	460	8.01	19.74	4.19	0.78	241.3 ± 27.5	Paragneiss
02-TG-15	N58°57'16.1"	W064°24'25.2"	357	4.76	103.84	47.07	0.59	203.9 ± 14.7	Paragneiss
02-TG-16	N58°57'27.5"	W064°19'43.6"	107	1.80	9.74	5.42	0.68	245.8 ± 37.5	Paragneiss
02-TG-17	N58°57'20.0"	W064°16'37.4"	111	1.15	7.61	6.41	0.68	198.2 ± 17.8	Granulite
02-TG-20	N59°00'49.4"	W064°02'49.1"	150	84.41	4.73	13.47	0.61	143.8 ± 5.2	Grnt-qtz-fspar gneiss
02-TG-24	N59°04'02.2"	W063°56'56.0"	75	125.95	9.39	8.96	0.67	134.4 ± 3.3	Grnt-qtz-fspar gneiss
02-TG-26	N59°02'43.7"	W063°47'34.6"	54	2.97	18.30	9.11	0.74	150.9 ± 10.3	Granulite
02-TG-28	N59°02'11.7"	W063°39'33.8"	32	0.04	1.32	1.12	0.65	134.0 ± 1.7	Granulite
02-TG-29	N59°01'46.4"	W063°36'08.4"	45	0.24	1.30	4.32	0.75	130.6 ± 3.0	Gneissic granite
02-TG-30	N59°03'55.8"	W063°27'00.1"	16	0.24	1.68	14.19	0.67	123.5 ± 18.8	Gneissic granite
02-TG-43	N59°11'05.8"	W063°57'12.5"	469	0.21	2.72	0.29	0.72	166.8 ± 24.2	Granulite
02-TG-61	N59°28'29.6"	W063°55'48.6"	477	0.06	1.02	0.92	0.72	78.7 ± 14.3	Granulite
02-TG-62	N59°29'28.1"	W063°57'35.2"	518	0.87	3.53	0.35	0.78	116.7 ± 4.4	Granulite
450 m N-S Transect									
02-TG-38	N58°58'53.1"	W063°46'44.0"	437	0.38	11.76	6.13	0.62	142.2 ± 12.2	Anorthosite
02-TG-40	N59°06'56.1"	W063°53'07.6"	479	2.72	8.19	15.94	0.77	147.5 ± 3.3	Granulite
02-TG-43	N59°11'05.8"	W063°57'12.5"	469	0.21	2.72	0.29	0.72	166.8 ± 24.2	Granulite
02-TG-44	N58°27'19.6"	W063°16'44.9"	369	348.43	17.04	12.70	0.64	332.6 ± 16.6	Meta-sediment
02-TG-45	N58°29'56.0"	W063°19'40.2"	364	0.25	3.28	4.11	0.59	316.4 ± 15.8	Granulite
02-TG-46	N58°33'37.5"	W063°18'54.3"	430	0.48	4.55	4.10	0.66	268.3 ± 25.2	Migmatite
02-TG-48	N58°38'01.1"	W063°29'53.2"	468	6.26	27.39	1.23	0.73	224.8 ± 13.3	Granulite
02-TG-61	N59°28'29.6"	W063°55'48.6"	477	0.06	1.02	0.92	0.72	78.7 ± 14.3	Granulite
02-TG-62	N59°29'28.1"	W063°57'35.2"	518	0.87	3.53	0.35	0.78	116.7 ± 4.4	Granulite
02-TG-66	N59°17'40.5"	W063°59'27.0"	497	0.24	3.01	1.18	0.71	129.2 ± 8.6	Granite gneiss
02-TG-68	N59°12'58.4"	W063°59'21.5"	458	1.15	15.40	1.57	0.69	127.8 ± 6.9	Granite gneiss
02-TG-73	N58°56'37.5"	W063°41'30.1"	424	0.32	3.19	6.01	0.73	97.5 ± 13.6	Granulite
02-TG-75	N58°49'18.3"	W063°33'07.1"	505	0.63	4.03	5.55	0.72	135.6 ± 3.7	Granulite
1000 m N-S Transect									
02-TG-50	N59°17'34.3"	W064°33'52.0"	1257	0.47	3.97	21.05	0.63	198.1 ± 2.1	Granulite
02-TG-51	N59°16'32.4"	W064°33'22.5"	1111	0.59	2.84	3.12	0.75	175.7 ± 3.2	Granulite
02-TG-52	N59°16'33.2"	W064°28'01.4"	1081	0.17	1.06	1.93	0.70	227.0 ± 0.6	Granulite
02-TG-53	N59°14'53.6"	W064°25'46.8"	1085	1.16	14.34	3.35	0,66	220.0 ± 12.0	Granulite
02-TG-54	N59°14'58.8"	W064°22'08.7"	1069	0.17	1.48	2.06	0.67	175.9 ± 8.6	Granulite
02-TG-55	N59°13'47.0"	W064°19'10.7"	1059	150.25	2.59	23.45	0.63	239.8 ± 12.0	Granulite
02-TG-56	N59°10'05.7"	W064°16'59.3"	1103	2.11	5.61	20.24	0.76	173.9 ± 29.1	Granulite
02-TG-58	N59°02'04.6"	W064°07'30.4"	1461	1.12	7.51	20.74	0.66	220.1 ± 19.1	Granulite
02-TG-59	N59°03'51.3"	W064°04'32.1"	1087	1.81	16.65	4.69	0.70	233.2 ± 56.9	Grnt-qtz-fspar gneiss
02-TG-60	N58°52'58.9"	W064°08'01.9"	1042	0.52	1.65	1.08	0.73	348.7 ± 17.4	Granulite
Mount D'Iberville									
02-TG-36	N58°59'44.5"	W063°45'21.4"	196	1.35	2.92	4.69	0.78	121.2 ± 8.2	Granulite
02-TG-37	N58°59'18.7"	W063°45'55.0"	383	0.32	4.45	10.45	0.67	123.6 ± 13.1	Granulite
02-TG-38	N58°58'53.1"	W063°46'44.0"	437	0.38	11.76	6.13	0.62	142.2 ± 12.2	Anorthosite
02-TG-39	N58°58'31.0"	W063°48'05.1"	644	1.73	22.83	8.22	0.66	143.1 ± 6.0	Granulite
02-TG-69	N58°57'56.8"	W063°48'02.1"	808	3.81	48.95	4.72	0.67	143.6 ± 7.2	Granulite
02-TG-70	N58°57'33.8"	W063°47'51.8"	945	0.22	3.69	13.19	0.65	140.5 ± 1.8	Granulite
02-TG-72	N58°56'18.3"	W063°45'43.9"	1383	0.49	11.01	11.44	0.63	158.2 ± 3.9	Granulite

REFERENCES

Balkwill, H.R., McMillan, N.J., MacLean, B., Williams, G.L., and Srivastava, S.P. 1990. Geology of the Labrador Shelf, Baffin Bay, and Davis Strait. In: Keen, M.J. and Williams, G.L. (eds.) Geology of the Continental Margin of Eastern Canada. Geological Survey of Canada, Geology of Canada, no. 2, p. 293-348 (also Geological Society of America, The Geology of North America, v. I-1).

Barron, E.J. 1983. A warm, equable Cretaceous: the nature of the problem. Earth Science Reviews, 19, p. 305-338.

Bell, R.E., Karner, G.D., and Steckler, M.S. 1988. Early Mesozoic rift basins of eastern North America and their gravity anomalies: the role of detachments during extensions. Tectonics, 7, p. 447-462.

Bishop, P. and Goldrick, G. 2000. Geomorphological evolution of the East Australian continental margin. In: Summerfield, M.A. (ed.) Geomorphology and Global Tectonics. John Wiley and Sons, New York, p. 225-254.

Bohannon, R.G., Naeser, C.W., Schmidt, D.L., and Zimmermann, R.A. 1989. The timing of uplift, volcanism, and rifting peripheral to the Red Sea: a case for passive rifting? Journal of Geophysical Research, 94, p. 1683-1701.

Brown, R.W., Gallagher, K., Gleadow, A.J.W., and Summerfield, M.A. 2000. Morphotectonic evolution on the South Atlantic margins of Africa and South America. In: Summerfield, M.A. (ed.) Geomorphology and Global Tectonics. John Wiley and Sons, New York, p. 255-281.

Brown, R.W., Summerfield, M.A., and Gleadow, A.J.W. 2002. Denudational history along a transect across the Drakensberg Escarpment of southern Africa derived from apatite fission track thermochronology. Journal of Geophysical Research, 107, B12, 2333, doi:10.1029/2001JB000745.

Chalmers, J.A., Larsen, L.M., and Pedersen, A.K. 1995. Widespread Paleocene volcanism around the northern North Atlantic and Labrador Sea: evidence for a large, hot, early plume head. Journal of the Geological Society, London, 152, p. 965-969.

Chalmers, J.A. and Laursen, K.H. 1995. Labrador Sea: the extent of continental crust and the timing of the start of seafloor spreading. Marine and Petroleum Geology, 12, p. 205-217.

Chalmers, J.A. 1997. The continental margin off southern Greenland: along-strike transition from an amagmatic to a volcanic margin. Journal of the Geological Society, London, 154, p. 571-576.

Chalmers, J.A. 2000. Offshore evidence for Neogene uplift in central West Greenland. Global and Planetary Change, 24, p. 311-318.

Chalmers, J.A. and Pulvertaft, T.C.R. 2001. Development of the continental margins of the Labrador Sea: a review. In: Wilson, R.C.L., Whitmarsh, R.B., and Froitzheim, N. (eds.) Non-Volcanic Rifting of Continental Margins: A Comparison from Land and Sea. Geological Society, London, Special Publications, 187, p. 77-105.

Cooke, H.C. 1929. Studies of the physiography of the Canadian Shield. Transactions of the Royal Society of Canada, 3(25), p. 91-120.

Costain, J.K. and Speer J.A. 1988. Heat flow and geothermal resource potential of the Atlantic Coastal Plain. In: Sheridan, R.E. and Grow, J.A. (eds.) The geology of North America, the Atlantic Continental Margin, U.S., p. 521-528. Decade of North American Geology Series, vol. I-2. Geological Society of America, Boulder, CO.

DeConto, R.M., Hay, W.W., Thompson, S.L., and Bergengren, J. 1999. Late Cretaceous climate and vegetation interactions; cold continental interior paradox. In: Barrera, E. and Johnson, C. (eds.) Evolution of the Cretaceous ocean-climate system. Geological Society of America, Special Paper 332, p. 391-406.

Ehlers, T.A. and Farley, K.A. 2003. Apatite (U-Th)/He Thermochronometry: methods and applications to problems in tectonics and surface processes. Earth and Planetary Science Letters, 206, p. 1-14.

Farley, K.A., Wolf, R.A., and Silver, L.T. 1996. The effect of long alpha-stopping distances on (U-Th)/He ages. Geochimica et Cosmochimica Acta, 60, p. 4223-4229.

Farley, K.A. 2000. Helium diffusion from apatite: General behavior as illustrated by Durango fluorapatite. Journal of Geophysical Research, 105, B2, p. 2903-2914.

Farley, K.A., Rusmore, M.E., Bogue, S.W. 2001. Post-10 Ma uplift and exhumation of the northern Coast Mountains, British Columbia. Geology, 29, p. 99-102.

Farley, K.A. 2002. (U-Th)/He Dating: Techniques, Calibrations, and Applications. In: Porcelli, D., Ballentine, C.J., and Wieler, R. (eds.) Noble gases in geochemistry and cosmochemistry. Reviews in Mineralogy and Geochemistry, 47, p. 819-843.

Farley, K.A. and Stockli, D.F. 2002. (U-Th)/He dating of phosphates: apatite, monazite, and xenotime. In: Kohn, M.J., Rakovan, J., and Hughes, J.M. (eds.) Phosphates: geochemical , geobiological, and materials importance, 48, p. 559-577.

Funck, T. and Louden, K.E. 1999. Wide-angle seismic transect across the Torngat Orogen, northern Labrador; evidence for a Proterozoic crustal root. Journal of Geophysical Research, B, Solid Earth and Planets, 104, p. 7,463-7,480.

Funck, T., Louden, K.E., Wardle, R.J., Hall, J., Hobro, J.W., Salisbury, M.H., and Muzzatti, A.M. 2000. Three-dimensional structure of the Torngat Orogen (NE Canada) from active seismic tomography. Journal of Geophysical Research, B, Solid Earth and Planets, 105, p. 23,403-23,420.

Gallagher, K., Hawkesworth, C.J., Mantovani, M.S.M. 1994. The denudation history of the onshore continental margin of SE Brazil inferred from apatite fission track data. Journal of Geophysical Research, 99, B9, p. 18117-18145.

Gallagher, K. and Brown, R. 1997. The onshore record of passive margin evolution. Journal of the Geological Society, London, 154, p. 451-457.

Gallagher, K., Brown, R., and Johnson, C. 1998. Fission track analysis and its applications to geological problems. Annual Review of Earth and Planetary Sciences, 26, p. 519-572.

Gilchrist, A.R., Kooi, H., and Beaumont, C. 1994. Post-Gondwana geomorphic evolution of southwestern Africa: implications for the controls on landscape development from observations and numerical experiments. Journal of Geophysical Research, 99, p. 12,211-12,228.

Gradstein, F.M. and Srivastava, S.P. 1980. Aspects of Cenozoic stratigraphy and paleoceanography of the Labrador Sea and Baffin Bay. Palaeogeography, Palaeoclimatology, Palaeoecology, 30, p. 261-295.

Grant, A.C. 1980. Problems with plate tectonics: the Labrador Sea. Bulletin of Canadian Petroleum Geology, 28, p. 252-278.

Grist, A.M., Reynolds, P.H., Zentilli, M., and Beaumont, C. 1992. The Scotian Basin offshore Nova Scotia: thermal history and provenance of sandstones, from apatite fission track analysis $^{40}Ar/^{39}Ar$ data. Canadian Journal of Earth Sciences, 29, p. 909-924.

Gunnell, Y. 2000. Apatite fission track thermochronology: an overview of its potential and limitations in geomorphology. Basin Research, 12, p. 115-132.

Hall, J., Louden, K.E., Funck, T., and Deemer, S. 2002. Geophysical characteristics of the continental crust along the Lithoprobe Eastern Canadian Shield Onshore-Offshore Transect (ECSOOT): a review. Canadian Journal of Earth Sciences, 39, p. 569-587.

Hass, C.H. 1997. Evolution of the North Atlantic Ocean; an overview. In: Hass, C.H and Kaminski, M.A. (eds.) Contributions to the micropaleontology and paleoceanography of the northern North Atlantic. Grzybowski Foundation Special Publication, 5, p. 1-14.

Hellinger, S.J. and Sclater, J.G. 1983. Some comments on two-layer extensional models for the evolution of sedimentary basins. Journal of Geophysical Research, B, 88, 10, p. 8251-8269.

House, M.A., Wernicke, B.P., and Farley, K.A. 1998. Dating topography of the Sierra Nevada, California, using apatite (U-Th)/He ages. Nature, 396, p. 66-69.

House, M.A., Wernicke, B.P., and Farley, .K.A. 2001. Paleo-geomorphology of the Sierra Nevada, California, from (U-Th)/He ages in apatite. American Journal of Science, 301, p. 77-102.

Japsen, P. and Chalmers, J.A. 2000. Neogene uplift and tectonics around the North Atlantic: overview. Global and Planetary Change, 24, p. 165-173.

Jenkins, W.A.M. 1984. Ordovician rocks in the Eastcan et al. Freydis B-87 and other wells in offshore Atlantic Canada. Canadian Journal of Earth Sciences, v. 21, p. 864-868.

Juez-Larré, J. and Andriessen, P.A.M. 2002. Post Late Paleozoic tectonism in the southern Catalan Coastal Ranges (NE Spain), assessed by apatite fission track analysis. Tectonophysics, 349, 113-129.

Kooi, H. and Beaumont, C. 1994. Escarpment evolution on high elevation rifted margins: insights derived from a surface processes model that combines diffusion, advection, and reaction. Journal of Geophysical Research, 99, p. 12,191-12,209.

Lawver L.A. and Müller R.D. 1994. Iceland hotspot track. Geology, 22, p. 311-314.

Lisker, F. 2002. Review of fission track studies in northern Victoria Land, Antarctica - passive margin evolution versus uplift of the Transantarctic Mountains. Tectonophysics, 349, 57-73.

Lister, G.S., Etheridge, M.A., and Symonds, P.A. 1986. Detachment faulting and the evolution of passive continental margins. Geology, 14, 3, p. 246-250.

Little, H.P. 1936. Ordovician fossils from Labrador. Science, 83, 2177, p. 268-269.

Mancktelow, N.S. and Grasemann, B. 1997. Time-dependent effects of heat advection and topography on cooling histories during erosion. Tectonophysics, 270, p. 167-195.

Marquette, G.C., Gray, J.T., Gosse, J.C., Courchesne, F., Stockli, L., Macpherson, G., and Finkel, R. 2004. Felsenmeer persistence under non-erosive ice in the Torngat and Kaumajet mountains, Quebec and Labrador, as determined by soil weathering and cosmogenic nuclide exposure dating. Canadian Journal of Earth Sciences, 41, p. 19-38.

McMillan, N.J. 1973. Shelves of Labrador Sea and Baffin Bay, Canada. In: McCrossan, R. G. (ed.) Future Petroleum Provinces of Canada. Canadian Society of Petroleum Geologists, Memoir 1, p. 473-517.

McWhae, J.R.H., Elie, R., Laughton, K.C., and Gunther, P.R. 1980. Stratigraphy and petroleum prospects of the Labrador Shelf. Bulletin of Canadian Petroleum Geology, 28, p. 460-488.

Ollier, C.D. 1984. Morphotectonics of continental margins with great escarpments. In: Morisawa, M. and Hack, J.T. (eds.) Tectonic Geomorphology. Allen and Unwin, London, p. 3-25.

Persano, C., Stuart, M.S., Bishop, B., Barfod, D.N. 2002. Apatite (U-Th)/He age constraints on the development of the Great Escarpment on the southeastern Australian passive margin. Earth and Planetary Science Letters, 200, 79-90.

Pik, R., Marty, B., Carignan, J., and Lavé, J. 2003. Stability of the Upper Nile drainage network (Ethiopia) deduced from (U–Th)/He thermochronometry: implications for uplift and erosion of the Afar plume dome. Earth and Planetary Science Letters, 215, p 73-88.

Piper, D.J.W., Mudie, P.J., Fader, G.B., Josenhans, H.W., MacLean, B. and Vilks, G. 1990. Quaternary geology. In: Keen, M.J. and Williams, G.L. (eds.) Geology of the Continental Margin of Eastern Canada. Geological Survey of Canada, Geology of Canada, no. 2, p. 475-607 (also Geological Society of America, The Geology of North America, v. I-1).

Rohrmann, M., Andriessen, P., and van der Beek, P. 1996. The relationship between basin and margin thermal evolution assessed by fission track thermochronology: an application to offshore Norway. Basin Research, 8, p. 45-64.

Spotila, J.A., Bank, G.C., Reiners, P.W., Naeser, C.W., Naeser, N.D., and Henika, B.S. 2004. Origin of the Blue Ridge escarpment along the passive margin of Eastern North America. Basin Research, 16, 41-63.

Srivastava, S.P. 1978. Evolution of the Labrador Sea and its bearing on the early evolution of the North Atlantic. Geophysical Journal of the Royal Astronomical Society, 52, 313-357.

Srivastava, S.P., Falconer, R.K.H., and MacLean B. 1980. Labrador Sea, Davis Strait, Baffin Bay: geology and geophysics - a review. In: Kerr J.W., Fergusson, A.J., and Machan, L.C. (eds.) Geology of the North Atlantic Borderlands. Canadian Society of Petroleum Geologists, 7, p. 333-398.

Staiger, J.K.W., Gosse, J.C., Johnson, J., Fastook, J., Gray, J., Stockli, D.F., Stockli, L., and Finkel, R. 2005. Quaternary relief generation by polythermal glacier ice: a field-calibrated glacial erosion model. Earth and Planetary Science Letters, in press.

Stockli, D.F., Farley, K.A., and Dumitru, T.A. 2000. Calibration of the apatite (U-Th)/He thermochronometer on an exhumed fault block, White Mountains, California. Geology, 28, p. 983-986.

Stockli, D.F., Linn, J.K., Walker, J.D., and Dumitru, T.A. 2001. Miocene unroofing of the Canyon Range during extension along the Sevier Desert Detachment, west central Utah. Tectonics, 20, p. 289-307.

Stockli, D.F., Surpless, B.E., Dumitru, T.A, and Farley, K.A. 2002. Thermochronological constraints on the timing and magnitude of Miocene and Pliocene extension in the central Wassuk Range, western Nevada. Tectonics, 21 (4), 1028, doi:10.1029/2001TC001295.

Stüwe, K., White, L., and Brown, R. 1994. The influence of eroding topography on steady-state isotherms - application to fission track analysis. Earth and Planetary Science Letters, 124, p.63-74.

Taylor, F.C. 1979. Reconnaissance geology of a part of the Precambrian shield, northeastern Quebec, northern Labrador and Northwest Territories. Geological Survey of Canada, Memoir 393.

Umpleby, D.C. 1979. Geology of the Labrador Shelf. Geological Survey of Canada Paper, 79-13, 34 pp.

van der Beek, P., Cloetingh, S., and Andriessen, P. 1994. Mechanisms of extensional basin formation and vertical motions at rift flanks: constraints from tectonic modeling and fission-track thermochronology. Earth and Planetary Science Letters, 121, p. 417-433.

Wardle, R.J., James, J., Gower, C.F., Ryan, B., Nunn, G.A.G., Kerr, A., Clark, T., Verpaelst, P., and Perreault, S. 2000. Geological map of the LITHOPROBE Eastern Canadian Shield Onshore-Offshore Transect (ECSOOT) area, Labrador and adjacent parts of Quebec, version 1.0. LITHOPROBE ECSOOT synthesis project (map).

Wardle, R.J., James, D.T., Scott, D.J., and Hall, J. 2002. The southeastern Churchill Province: synthesis of a Paleoproterozoic transpressional orogen. Canadian Journal of Earth Sciences, 39, p. 639-663.

Wares, R.P. and Goutier, J. 1990. Deformational style in the foreland of the New Quebec Orogen. Geoscience Canada, 17, 244-249.

Wolf, R.A., Farley, K.A., Silver, L.T. 1996. Helium diffusion and low-temperature thermochronometry of apatite. Geochimica et Cosmochimica Acta, 60, p. 4231-4240.

Wolf, R.A., Farley, K.A., and Kass, D.M. 1998. Modeling of the temperature sensitivity of the apatite (U-Th)/ He thermochronometer. Chemical Geology, 148, p. 105-114.

APPENDIX A:

Description of Analytical Methods

Mineral Separation

Separation was done at the University of Kansas Geology Mineral Separation Facilities. Samples were crushed using a sledge hammer and a jaw crusher. A hand size rock fragment was saved from each sample for future reference. The remaining fragments were further crushed and grinded using a 21 cm disc mill until the entire sample was converted to sand. The average sand grain size ranged between 500 and 50 microns.

A pyramid table (similar to a Wilfley table) was used to separate the "light" from the "heavy" minerals. From the minerals seen after the pyramid table step, the "heavy" portion can be considered to have a specific gravity (SG) greater than 2.8. The "heavy" portion of each sample was separated using bromoform (SG = 2.9), which removed mostly biotite. A Frantz Isodynamic Magnetic Separator® was used to remove magnetic and high paramagnetic material (usually magnetite, garnet, biotite, and monazite) leaving behind mostly zircon and apatite. Concentrates of zircon (SG $\approx$ 4.6) and apatite (SG $\approx$ 3.2) were separated using methylene iodide (SG = 3.32).

Sample Preparation

Analyses were performed on euhedral to subhedral and optically inclusion-free apatite grains that were hand picked using a Nikon SMZ-U stereomicroscope with a rotating stage. All grains were digitally photographed using a Nikon digital ColorView® camera and all digital pictures were archived. AnalySIS® imaging software was used to morphometrically measure each grain. The average grain dimensions for this study's apatites were 60±15 μm in radius and 150±75 μm in length.

Picked apatite grains from each sample were arranged in three to four groups of 3 to 5 grains according to size. Each group was inserted in a platinum packet of 1 mm by 1 mm.

Laser Helium Extraction and Mass Analysis

The University of Kansas Geology (U-Th)/He Extraction Line was used to extract helium from all the apatite samples. Each platinum packet was placed in a copper planchet that holds 36 packets. Each packet was heated separately at approximately 1000°C using a Nd-YAG laser beam (1064 nm, <1 W, continuous wave, US Laser Corp.) for 4.5 minutes. The extracted ^{4}He was collected on a high vacuum metal line, spiked with ^{3}He, and then analyzed on a Blazers Prisma QMS-200 quadrupole mass spectrometer to measure the $^{3}He/^{4}He$ ratio.

The platinum packets containing apatite were retrieved from the vacuum chamber and transferred into teflon beakers. Into each beaker, 1 ml of a 20% HNO_3

spiked solution (^{230}Th + ^{235}U) was added for dissolution. The solution was heated at approximately 80°C for 1 hour to insure complete dissolution. After they cooled to room temperature, 1 ml of milliQ water was added to each beaker. The solutions were then analyzed for U and Th at the University of Kansas Plasma Analytical Laboratory using a VG PlasmaQuad II+XS Inductively Coupled Plasma Mass Spectrometer (ICP-MS).

APPENDIX B:

Summary of All Apatite (U-Th)/He Data from the Torngat Mountains

Sample	Latitude, North	Longitude, West	Elevation, m	He, ncc	U, ppm	Th, ppm	Correction factor, Ft	Corrected age (Ma) ± 2σ	Rock Type
E-W Transect									
02TG01-A	N58°59'27.2"	W064°43'47.5"	463	0.18	0.93	6.69	0.65	233.5 ± 11.7	Granite gneiss
02TG01-B				0.44	5.31	5.53	0.71	162.1 ± 8.1	
02TG01-C				0.20	1.45	5.44	0.67	177.9 ± 8.9	
02TG01-D				0.14	1.89	0.27	0.74	164.2 ± 8.2	
02TG02-A	N58°58'07.5"	W064°32'58.2"	446	2.09	20.48	47.96	0.66	193.4 ± 9.7	Paragneiss
02TG02-B				1.31	18.75	59.51	0.61	185.5 ± 9.3	
02TG02-D				1.69	12.22	22.01	0.72	162.5 ± 8.1	
02TG02-E				3.88	22.38	72.06	0.69	193.2 ± 9.7	
02TG03-A	N58°58'06.7"	W064°33'04.9"	438	4.93	11.16	1.54	0.80	175.8 ± 8.8	Paragneiss
02TG03-B				2.30	4.47	2.20	0.80	265.4 ± 13.3	
02TG03-C				2.20	5.32	1.86	0.73	514.4 ± 25.7	
02TG03-D				1.75	7.26	1.48	0.69	428.4 ± 21.4	
02TG04-A	N58°58'37.4"	W064°34'16.4"	418	0.31	8.47	0.80	0.64	132.9 ± 6.6	Granulite
02TG04-B				1.08	14.26	0.96	0.67	141.2 ± 7.1	
02TG04-C				1.39	12.75	0.65	0.66	179.1 ± 9.0	
02TG04-D				1.14	10.69	0.73	0.71	154.3 ± 7.7	
02TG05-A	N58°58'47.9"	W064°36'37.5"	428	2.38	10.03	13.00	0.75	173.5 ± 8.7	Granite gneiss
02TG05-B				1.74	6.97	15.19	0.74	164.5 ± 8.2	
02TG05-C				0.93	4.08	11.18	0.72	163.1 ± 8.2	
02TG05-D				1.04	4.57	10.67	0.73	168.5 ± 8.4	
02TG06-A	N58°58'28.3"	W064°40'40.3"	437	0.40	2.96	3.37	0.72	137.8 ± 6.9	Granite gneiss
02TG06-B				1.01	4.49	6.14	0.74	180.1 ± 9.0	
02TG06-C				0.22	2.58	4.84	0.69	123.3 ± 6.2	
02TG06-D				1.30	4.03	3.54	0.78	167.5 ± 8.4	
02TG07-A	N58°57'48.2"	W064°46'48.9"	490	0.42	7.66	3.68	0.64	145.2 ± 7.3	Granite gneiss
02TG07-B				1.77	9.38	0.77	0.72	199.0 ± 10.0	
02TG07-C				2.51	11.29	4.72	0.80	120.1 ± 6.0	
02TG07-D				0.47	6.54	1.59	0.68	133.5 ± 6.7	
02TG08-A	N58°58'03.4"	W064°49'24.9"	552	24.98	68.86	8.36	0.81	201.0 ± 10.1	Granite gneiss
02TG08-B				8.36	18.62	2.17	0.80	213.9 ± 10.7	
02TG08-C				27.26	29.52	1.20	0.83	244.8 ± 12.2	
02TG08-D				26.11	42.15	10.18	0.82	190.6 ± 9.5	
02TG12-A	N59°01'20.2"	W065°03'54.3"	301	1.79	11.35	4.33	0.72	159.1 ± 8.0	Granite gneiss
02TG12-B				7.01	16.55	6.18	0.79	162.2 ± 8.1	
02TG12-C				5.62	15.97	7.87	0.78	157.4 ± 7.9	
02TG12-D				4.98	14.07	13.19	0.73	181.2 ± 9.1	
02TG14-A	N58°56'52.4"	W064°28'29.6"	460	5.42	13.90	2.49	0.79	213.0 ± 10.6	Paragneiss
02TG14-B				4.72	15.51	3.17	0.75	267.9 ± 13.4	
02TG14-C				13.91	14.78	1.53	0.81	346.5 ± 17.3	
02TG14-D				13.91	29.80	6.92	0.79	243.2 ± 12.2	
02TG15-A	N58°57'16.1"	W064°24'25.2"	357	4.26	117.65	88.17	0.55	225.7 ± 11.3	Paragneiss
02TG15-B				7.01	107.80	25.95	0.64	194.3 ± 9.7	
02TG15-C				5.00	96.71	25.68	0.62	200.0 ± 10.0	
02TG15-D				2.75	93.21	48.49	0.55	195.7 ± 9.8	
02TG16-A	N58°57'27.5"	W064°19'43.6"	107	0.90	5.85	4.98	0.67	286.8 ± 14.3	Paragneiss
02TG16-B				0.42	6.08	7.89	0.63	213.3 ± 10.7	
02TG16-C				4.08	17.30	3.37	0.75	237.4 ± 11.9	
02TG16-D				1.25	7.88	6.49	0.63	421.5 ± 21.1	
02TG17-B	N58°57'20.0"	W064°16'37.4"	111	2.54	8.46	2.28	0.71	349.6 ± 17.5	Granulite
02TG17-C				1.82	6.93	5.57	0.73	210.8 ± 10.5	
02TG17-D				0.48	8.28	7.24	0.62	185.6 ± 9.3	
02TG18-A	N58°58'30.0"	W064°14'12.8"	110	1.34	5.55	13.29	0.62	643.5 ± 32.2	Granulite
02TG18-A1				793.28	8.46	12.31	0.65	836.6 ± 41.8	
02TG18-B				4.51	9.57	14.85	0.68	716.8 ± 35.8	
02TG18-B1				316.21	9.34	14.09	0.65	308.5 ± 15.4	
02TG18-C				3.30	7.94	14.93	0.69	516.6 ± 25.8	
02TG19-A	N58°59'17.4"	W064°09'46.8"	78	8.00	0.10	0.61	0.69	375.7 ± 18.8	Granulite
02TG19-B				82.21	0.07	0.83	0.73	2965.5 ± 148.3	
02TG19-C				43.86	0.08	2.25	0.71	817.3 ± 40.9	
02TG20-A	N59°00'49.4"	W064°02'49.1"	150	67.30	4.16	8.81	0.61	145.1 ± 7.3	Grnt-qtz-fspar gneiss
02TG20-B				83.41	4.80	18.19	0.54	138.1 ± 6.9	
02TG22-A	N59°01'39.2"	W063°59'12.8"	167	0.40	-0.01	0.40	0.77	52.3 ± 2.6	Grnt-qtz-fspar gneiss
02TG22-B				841.45	1.77	1.13	0.77	1772.3 ± 88.6	
02TG22-C				1.03	0.15	1.98	0.65	21.1 ± 1.1	

APPENDIX B:

(CONTINUED)

Sample	Latitude, North	Longitude, West	Elevation, m	He, ncc	U, ppm	Th, ppm	Correction factor, Ft	Corrected age (Ma) ± 2σ	Rock Type
02TG24-A	N59°04'02.2"	W063°56'56.0"	75	123.41	9.78	3.60	0.72	131.5 ± 6.6	Grnt-qtz-fspar gneiss
02TG24-B				120.10	10.64	5.72	0.59	138.0 ± 6.9	
02TG24-C				134.34	7.73	17.56	0.69	133.7 ± 6.7	
02TG26-A	N59°02'43.7"	W063°47'34.6"	54	2.82	16.55	7.44	0.74	162.3 ± 8.1	Granulite
02TG26-B				4.07	21.66	11.24	0.76	143.6 ± 7.2	
02TG26-C				2.02	19.44	8.93	0.72	156.8 ± 7.8	
02TG26-D				2.98	15.56	8.84	0.76	141.0 ± 7.0	
02TG27-A	N59°00'58.0"	W063°43'52.7"	17	8.30	7.31	12.89	0.75	799.8 ± 40.0	Granulite
02TG27-A1				2.88	3.95	2.78	0.74	610.2 ± 30.5	
02TG27-B				1.60	3.10	6.20	0.69	741.1 ± 37.1	
02TG27-B1				4.58	4.97	0.73	0.72	1102.7 ± 55.1	
02TG27-C				1.17	4.67	9.48	0.69	333.8 ± 16.7	
02TG27-C1				2.03	4.92	1.13	0.71	587.0 ± 29.4	
02TG27-D				2.22	3.29	9.38	0.61	1437.1 ± 71.9	
02TG27-D1				5.05	1.78	1.15	0.73	2043.3 ± 102.2	
02TG27-E				6.28	5.39	4.00	0.75	1233.3 ± 61.7	
02TG28-A	N59°02'11.7"	W063°39'33.8"	32	0.04	1.01	0.86	0.68	135.2 ± 6.8	Granulite
02TG28-B				0.01	0.71	1.58	0.60	91.9 ± 4.6	
02TG28-C				0.04	1.63	1.37	0.61	132.9 ± 6.6	
02TG29-A	N59°01'46.4"	W063°36'08.4"	45	0.20	1.19	4.81	0.74	132.7 ± 6.6	Gneissic granite
02TG29-B				13.11	1.63	4.18	0.75	207.2 ± 10.4	
02TG29-C				0.28	1.42	3.84	0.76	128.5 ± 6.4	
02TG29-D				26.43	1.46	1.99	0.81	172.3 ± 8.6	
02TG30-A	N59°03'55.8"	W063°27'00.1"	16	0.22	1.62	16.02	0.63	143.0 ± 7.2	Gneissic granite
02TG30-B				0.37	1.63	10.45	0.75	134.5 ± 6.7	
02TG30-C				0.11	0.79	15.57	0.61	115.4 ± 5.8	
02TG30-D				0.27	2.67	14.73	0.70	101.3 ± 5.1	
02TG43-A	N59°11'05.8"	W063°57'12.5"	469	0.20	2.87	0.11	0.76	183.9 ± 9.2	Granulite
02TG43-B				0.22	2.57	0.47	0.69	149.7 ± 7.5	
02TG43-C				0.44	3.02	0.20	0.71	240.1 ± 12.0	
02TG43-D				0.61	3.16	2.08	0.68	292.4 ± 14.6	
02TG61-A	N59°28'29.6"	W063°55'48.6"	477	0.09	0.97	0.60	0.75	91.0 ± 4.6	Granulite
02TG61-B				0.07	1.49	1.17	0.71	82.2 ± 4.1	
02TG61-C				0.03	0.60	1.00	0.70	62.9 ± 3.1	
02TG62-A	N59°29'28.1"	W063°57'35.2"	518	0.55	3.72	0.33	0.76	113.0 ± 5.7	Granulite
02TG62-B				1.55	3.94	0.28	0.82	115.4 ± 5.8	
02TG62-C				0.51	2.94	0.42	0.77	121.6 ± 6.1	
450 m N-S Transect									
02TG38-A	N58°58'53.1"	W063°46'44.0"	437	0.20	10.36	6.42	0.56	154.3 ± 7.7	Anorthosite
02TG38-B				0.36	10.38	7.21	0.64	140.4 ± 7.0	
02TG38-C				0.28	12.18	4.89	0.61	126.0 ± 6.3	
02TG38-D				0.69	14.12	6.00	0.68	148.2 ± 7.4	
02TG40-A	N59°06'56.1"	W063°53'07.6"	479	1.96	7.05	12.90	0.75	186.5 ± 9.3	Granulite
02TG40-B				3.79	7.23	14.82	0.75	301.6 ± 15.1	
02TG40-C				3.65	7.75	12.08	0.80	145.2 ± 7.3	
02TG40-D				1.80	8.64	19.80	0.74	149.8 ± 7.5	
02TG42-A				2.95	17.14	14.39	0.60	680.6 ± 34.0	Granulite
02TG42-B				7.75	13.68	10.74	0.70	767.7 ± 38.4	
02TG42-C				3.64	8.19	1.49	0.68	919.4 ± 46.0	
02TG43-A	N59°11'05.8"	W063°57'12.5"	469	0.20	2.87	0.11	0.76	183.9 ± 9.2	Granulite
02TG43-B				0.22	2.57	0.47	0.69	149.7 ± 7.5	
02TG43-C				0.44	3.02	0.20	0.71	240.1 ± 12.0	
02TG43-D				0.61	3.16	2.08	0.68	292.4 ± 14.6	
02TG44-A	N58°27'19.6"	W063°16'44.9"	369	3.00	9.89	7.51	0.73	449.9 ± 22.5	Meta-sediment
02TG44-A1				467.14	14.91	15.68	0.57	353.5 ± 17.7	
02TG44-B				2.85	11.26	3.34	0.75	529.7 ± 26.5	
02TG44-B1				504.95	18.80	8.34	0.64	308.1 ± 15.4	
02TG44-C				2.18	22.47	22.62	0.70	283.2 ± 14.2	
02TG44-C1				419.44	12.00	4.16	0.67	385.8 ± 19.3	
02TG45-A	N58°29'56.0"	W063°19'40.2"	364	0.25	3.28	4.11	0.59	316.4 ± 15.8	Granulite
02TG45-A1				187.98	2.30	3.72	0.64	727.6 ± 36.4	
02TG45-B				0.32	1.79	0.93	0.63	651.6 ± 32.6	
02TG45-B1				149.72	4.09	4.53	0.65	362.4 ± 18.1	
02TG45-C				0.70	2.45	1.83	0.62	886.7 ± 44.3	

APPENDIX B:

(CONTINUED)

Sample	Latitude, North	Longitude, West	Elevation, m	He, ncc	U, ppm	Th, ppm	Correction factor, Ft	Corrected age (Ma) ± 2σ	Rock Type
02TG45-C1				98.71	1.59	2.51	0.68	525.7 ± 26.3	
02TG46-A	N58°33'37.5"	W063°18'54.3"	430	0.50	5.19	6.66	0.62	286.4 ± 14.3	Migmatite
02TG46-B				0.48	4.36	0.81	0.68	239.5 ± 12.0	
02TG46-C				0.45	4.10	4.84	0.68	279.1 ± 14.0	
02TG48-A	N58°38'01.1"	W063°29'53.2"	468	6.83	21.68	0.59	0.77	212.5 ± 10.6	Granulite
02TG48-B				2.20	32.34	0.99	0.64	223.1 ± 11.2	
02TG48-C				9.76	28.16	2.10	0.79	238.9 ± 11.9	
02TG61-A	N59°28'29.6"	W063°55'48.6"	477	0.09	0.97	0.60	0.75	91.0 ± 4.6	Granulite
02TG61-B				0.07	1.49	1.17	0.71	82.2 ± 4.1	
02TG61-C				0.03	0.60	1.00	0.70	62.9 ± 3.1	
02TG62-A	N59°29'28.1"	W063°57'35.2"	518	0.55	3.72	0.33	0.76	113.0 ± 5.7	Granulite
02TG62-B				1.55	3.94	0.28	0.82	115.4 ± 5.8	
02TG62-C				0.51	2.94	0.42	0.77	121.6 ± 6.1	
02TG66-A	N59°17'40.5"	W063°59'27.0"	497	0.20	2.99	1.63	0.68	138.7 ± 6.9	Granite gneiss
02TG66-B				0.26	3.24	1.08	0.72	126.6 ± 6.3	
02TG66-C				0.25	2.80	0.81	0.73	122.1 ± 6.1	
02TG68-A	N59°12'58.4"	W063°59'21.5"	458	1.60	19.29	1.90	0.71	125.7 ± 6.3	Granite gneiss
02TG68-B				0.75	17.14	1.46	0.64	122.2 ± 6.1	
02TG68-C				1.10	9.77	1.36	0.72	135.5 ± 6.8	
02TG73-A	N58°56'37.5"	W063°41'30.1"	424	0.46	2.61	3.89	0.76	107.4 ± 5.4	Granulite
02TG73-B				0.17	3.14	4.50	0.72	81.9 ± 4.1	
02TG73-C				0.34	3.81	9.63	0.71	103.1 ± 5.2	
02TG75-A	N58°49'18.3"	W063°33'07.1"	505	1.27	4.61	6.41	0.71	295.8 ± 14.8	Granulite
02TG75-B				0.83	3.86	5.74	0.75	133.0 ± 6.6	
02TG75-C				0.42	4.21	5.36	0.69	138.3 ± 6.9	
1000 m N-S Transect									
02TG50-A	N59°17'34.3"	W064°33'52.0"	1257	0.67	4.59	25.59	0.66	198.3 ± 9.9	Granulite
02TG50-B				0.36	3.48	17.22	0.63	200.1 ± 10.0	
02TG50-C				0.37	3.83	20.35	0.61	196.0 ± 9.8	
02TG51-A	N59°16'32.4"	W064°33'22.5"	1111	0.91	2.88	5.31	0.78	177.9 ± 8.9	Granulite
02TG51-B				0.59	3.71	4.39	0.73	225.9 ± 11.3	
02TG51-C				0.27	2.79	0.93	0.72	173.4 ± 8.7	
02TG52-A	N59°16'33.2"	W064°28'01.4"	1081	0.32	0.51	0.50	0.64	1733.2 ± 86.7	Granulite
02TG52-B				0.13	0.71	1.63	0.71	227.4 ± 11.4	
02TG52-C				0.22	1.41	2.23	0.69	226.5 ± 11.3	
02TG53-A	N59°14'53.6"	W064°25'46.8"	1085	1.88	19.89	5.53	0.68	229.9 ± 11.5	Granulite
02TG53-B				0.53	7.64	1.50	0.67	206.7 ± 10.3	
02TG53-C				1.06	15.49	3.01	0.63	223.2 ± 11.2	
02TG54-A	N59°14'58.8"	W064°22'08.7"	1069	0.08	1.58	2.31	0.61	182.0 ± 9.1	Granulite
02TG54-B				0.26	1.39	1.82	0.74	169.8 ± 8.5	
02TG54-C				0.16	1.63	1.65	0.64	286.7 ± 14.3	
02TG55-A	N59°13'47.0"	W064°19'10.7"	1059	2.67	2.59	23.06	0.70	549.0 ± 27.5	Granulite
02TG55-A1				150.25	2.59	23.45	0.63	239.8 ± 12.0	
02TG55-B				1.79	2.12	24.47	0.60	1205.3 ± 60.3	
02TG55-B1				369.92	4.14	31.36	0.60	435.7 ± 21.8	
02TG55-C				5.85	2.38	25.26	0.69	1274.9 ± 63.7	
02TG55-C1				286.34	3.37	25.15	0.61	410.4 ± 20.5	
02TG56-A	N59°10'05.7"	W064°16'59.3"	1103	2.13	5.12	17.55	0.76	194.4 ± 9.7	Granulite
02TG56-B				1.09	3.80	10.09	0.74	221.1 ± 11.1	
02TG56-C				2.09	6.09	22.94	0.76	153.3 ± 7.7	
02TG57-A	N59°06'05.7"	W064°16'11.4"	1000	6.72	5.48	25.46	0.65	1922.3 ± 96.1	Granulite
02TG57-B				0.00	0.03	3.52	0.71	6.4 ± 0.3	
02TG57-C				0.00	-0.01	3.95	0.61	5.0 ± 0.3	
02TG58-A	N59°02'04.6"	W064°07'30.4"	1461	1.42	8.21	22.52	0.66	234.5 ± 11.7	Granulite
02TG58-B				0.82	8.56	23.40	0.60	227.3 ± 11.4	
02TG58-C				1.12	5.77	16.29	0.71	198.5 ± 9.9	
02TG59-A	N59°03'51.3"	W064°04'32.1"	1087	2.45	15.35	5.35	0.75	192.9 ± 9.6	Grnt-qtz-fspar gneiss
02TG59-B				1.17	17.96	4.02	0.65	273.4 ± 13.7	
02TG59-C				2.27	15.15	2.42	0.68	424.9 ± 21.2	
02TG60-A	N58°52'58.9"	W064°08'01.9"	1042	0.52	1.65	1.08	0.73	348.7 ± 17.4	Granulite
02TG60-A1				171.72	2.07	1.71	0.66	815.0 ± 40.8	
02TG60-B				0.44	1.90	2.21	0.66	444.0 ± 22.2	
02TG60-B1				116.52	1.55	2.33	0.69	636.6 ± 31.8	
02TG60-C				0.77	1.68	1.33	0.72	589.6 ± 29.5	
02TG60-C1				76.39	1.21	0.83	0.73	586.9 ± 29.3	

APPENDIX B:

(CONTINUED)

Sample	Latitude, North	Longitude, West	Elevation, m	He, ncc	U, ppm	Th, ppm	Correction factor, Ft	Corrected age (Ma) ± 2σ	Rock Type
Mount D'Iberville									
02TG27-A	N59°00'58.0"	W063°43'52.7"	17	8.30	7.31	12.89	0.75	799.8 ± 40.0	Granulite
02TG27-A1				2.88	3.95	2.78	0.74	610.2 ± 30.5	
02TG27-B				1.60	3.10	6.20	0.69	741.1 ± 37.1	
02TG27-B1				4.58	4.97	0.73	0.72	1102.7 ± 55.1	
02TG27-C				1.17	4.67	9.48	0.69	333.8 ± 16.7	
02TG27-C1				2.03	4.92	1.13	0.71	587.0 ± 29.4	
02TG27-D				2.22	3.29	9.38	0.61	1437.1 ± 71.9	
02TG27-D1				5.05	1.78	1.15	0.73	2043.3 ± 102.2	
02TG27-E				6.28	5.39	4.00	0.75	1233.3 ± 61.7	
02TG36-A	N58°59'44.5"	W063°45'21.4"	196	1.91	3.76	5.06	0.80	114.1 ± 5.7	Granulite
02TG36-B				0.81	2.56	5.41	0.77	116.1 ± 5.8	
02TG36-C				1.91	3.10	3.13	0.80	132.4 ± 6.6	
02TG36-D				0.76	2.26	5.17	0.76	122.3 ± 6.1	
02TG37-A	N58°59'18.7"	W063°45'55.0"	383	0.28	4.69	7.75	0.67	113.8 ± 5.7	Granulite
02TG37-B				0.19	4.96	14.19	0.62	111.1 ± 5.6	
02TG37-C				0.44	3.69	9.35	0.70	137.6 ± 6.9	
02TG37-D				0.38	4.46	10.50	0.69	131.9 ± 6.6	
02TG38-A	N58°58'53.1"	W063°46'44.0"	437	0.20	10.36	6.42	0.56	154.3 ± 7.7	Anorthosite
02TG38-B				0.36	10.38	7.21	0.64	140.4 ± 7.0	
02TG38-C				0.28	12.18	4.89	0.61	126.0 ± 6.3	
02TG38-D				0.69	14.12	6.00	0.68	148.2 ± 7.4	
02TG39-A	N58°58'31.0"	W063°48'05.1"	644	1.03	24.78	12.82	0.64	138.7 ± 6.9	Granulite
02TG39-B				0.74	24.75	5.88	0.61	140.7 ± 7.0	
02TG39-C				3.42	18.95	5.97	0.75	149.9 ± 7.5	
02TG39-D				1.77	18.17	16.97	0.68	174.6 ± 8.7	
02TG69-A	N58°57'56.8"	W063°48'02.1"	808	5.90	38.32	3.40	0.79	166.4 ± 8.3	Granulite
02TG69-B				5.98	85.73	3.39	0.66	176.7 ± 8.8	
02TG69-C				2.62	48.09	1.30	0.65	172.0 ± 8.6	
02TG69-D				0.74	23.64	10.81	0.57	143.6 ± 7.2	
02TG70-A	N58°57'33.8"	W063°47'51.8"	945	0.25	2.28	8.33	0.72	111.0 ± 5.6	Granulite
02TG70-B				0.26	4.54	11.30	0.66	139.3 ± 7.0	
02TG70-C				0.15	4.24	19.94	0.59	141.8 ± 7.1	
02TG71-A	N58°57'21.0"	W063°47'40.6"	1129	0.22	0.09	4.47	0.70	440.1 ± 22.0	Granulite
02TG71-A1				0.82	2.52	1.15	0.69	487.3 ± 24.4	
02TG71-B				4.58	2.93	3.91	0.74	1551.0 ± 77.6	
02TG71-B1				1.59	1.76	2.59	0.73	1056.5 ± 52.8	
02TG71-C				2.84	1.59	3.08	0.75	1340.7 ± 67.0	
02TG71-C1				0.58	2.02	4.87	0.65	591.9 ± 29.6	
02TG72-A	N58°56'18.3"	W063°45'43.9"	1383	0.45	7.63	11.14	0.67	160.9 ± 8.0	Granulite
02TG72-B				0.52	14.39	11.73	0.59	155.4 ± 7.8	
02TG72-C				2.38	54.59	30.95	0.63	206.5 ± 10.3	
02TG72-D				10.56	6.18	10.31	0.67	2681.5 ± 134.1	
Mount Inuit									
02TG35-A	N59°04'55.1"	W064°00'55.4"	251	0.00	-0.02	0.49	0.70	13.8 ± 0.7	Grnt-qtz-fspar gneiss
02TG35-B				0.00	0.00	0.31	0.74	6.9 ± 0.3	
02TG35-C				0.00	0.23	0.43	0.71	1.8 ± 0.1	
02TG35-D				2.13	32.38	9.25	0.73	260.3 ± 13.0	
02TG58-A	N59°02'04.6"	W064°07'30.4"	1461	1.42	8.21	22.52	0.66	234.5 ± 11.7	Granulite
02TG58-B				0.82	8.56	23.40	0.60	227.3 ± 11.4	
02TG58-C				1.12	5.77	16.29	0.71	198.5 ± 9.9	
02TG59-A	N59°03'51.3"	W064°04'32.1"	1087	2.45	15.35	5.35	0.75	192.9 ± 9.6	Grnt-qtz-fspar gneiss
02TG59-B				1.17	17.96	4.02	0.65	273.4 ± 13.7	
02TG59-C				2.27	15.15	2.42	0.68	424.9 ± 21.2	